Role of the signalling lymphocytic activation molecule (SLAM)–associated protein (SAP) in the host response and intra-host evolution of SARS-CoV-2

By

Nathan Marko Markarian

Department of Human Genetics, Faculty of Medicine, and Health Sciences

McGill University, Montreal, Quebec, Canada

June 2023

A thesis submitted to McGill University in partial fulfillment of the requirement of the degree of

Master of Science (M.Sc.)

Table of Contents

Abstract

With about 7 million cumulative deaths, the COVID-19 pandemic continues, giving rise to different variants of concerns (VOCs) with the potential to escape existing treatments. Indeed, there are several reports of de novo structural variants in different SARS-CoV-2 proteins that arose in immunodeficient patients with chronic SARS-CoV-2 infection and receiving treatment. Some have hypothesized that existing SARS-CoV-2 variants of concern (VOCs) such as the Omicron variants may have arisen from selection pressures occurring during chronic infections. Previously, in cases of X-linked lymphoproliferative (XLP) syndrome, the signaling lymphocyte activation molecule (SLAM)-associated protein (SAP) was first identified as the affected protein leading to a defective immune system. Indeed, SAP-deficient mice also recapitulate multiple immune defects of XLP patients, including impaired $CD8^+$ and NK cell cytotoxicity, lack of circulating NKT cells and generation of long-term humoral immunity. In addition, the mouse K18-ACE2 transgenic model of SARS-CoV-2 infection replicates key features of COVID-19, which is dependent in cell-mediated immunity. To address the importance of NK and $CD8^+$ T cell immunodeficiency in SARS-CoV-2 infections and intra-host viral evolution, we have produced male K18-hACE2 transgenic/SAP hemizygous (SAP KO) mice and male K18-hACE2 (SAP WT) transgenic offspring and infected them with an earlier strain of SARS-CoV-2. Infection dynamics were first investigated, finding similar clinical and virological findings for both SAP KO and WT. However, a differential expression of immune genes was found in SAP KO compared to WT, with a trend towards increased mouse interferon γ (IFNγ) and a significant increase in granzyme B, perforin 1 and CD8α expression in SAP KO infected mice. Finally, serial passaging of SARS-CoV-2 in both SAP KO and WT mice was performed and novel variants were screened by RNA sequencing, revealing differences in the mutational profile of SAP KO passaged viruses compared to SAP WT.

These results suggest a differential immune response and viral selection pressures found in SAP deficient mice infected with SARS-CoV-2.

Résumé

Avec environ 7 millions de décès cumulés, la pandémie de COVID-19 se poursuit, donnant lieu à différentes variants de préoccupations (VOC) susceptibles de résister aux traitements existants. En effet, de nombreux rapports font état de variants structurels de novo dans différentes protéines du SRAS-CoV-2 qui sont apparus chez des patients immunodéficients atteints d'une infection chronique par le SRAS-CoV-2 et recevant un traitement. Certains ont émis l'hypothèse que les variants préoccupants (VOC) du SRAS-CoV-2, tels que les variants Omicron, pourraient être le résultat de pressions de sélection exercées lors d'infections chroniques. Auparavant, dans les cas de syndrome lymphoprolifératif lié à l'X (XLP), la protéine associée à la molécule d'activation des lymphocytes de signalisation (SLAM) a été identifiée pour la première fois comme la protéine affectée conduisant à un déficit immunitaire. En effet, les souris déficientes en SAP récapitulent plusieurs défauts immunitaires des patients XLP, notamment une cytotoxicité altérée des cellules $CD8^+$ et NK, l'absence de cellules NKT circulantes et la génération d'une immunité humorale à long terme. En outre, le modèle transgénique K18-ACE2 d'infection par le SRAS-CoV-2 reproduit les principales caractéristiques de COVID-19, qui dépend de l'immunité à médiation cellulaire. Pour étudier l'importance de l'immunodéficience des cellules NK et T $CD8^+$ dans les infections par le SRAS-CoV-2 et l'évolution virale intra-hôte, nous avons produit des souris mâles transgéniques K18-hACE2/SAP hémizygotes (SAP KO) et des descendants transgéniques K18-hACE2 (SAP WT) et les avons infectés avec une souche antérieure du SRAS-CoV-2. La dynamique de l'infection a d'abord été étudiée et les résultats cliniques et virologiques ont été similaires pour les souris SAP KO et WT. Cependant, une expression différentielle des gènes immunitaires a été observée chez les souris SAP KO par rapport aux souris WT, avec une tendance à l'augmentation de l'interféron γ (IFNγ), du granzyme B, de la perforine 1 et de l'expression du

CD8α chez les souris infectées par le SAP KO. Enfin, le passage en série du SARS-CoV-2 chez les souris SAP KO et WT a été effectué et de nouveaux variants ont été recherchés par séquençage de l'ARN, révélant des différences dans le profil mutationnel des virus passés par SAP KO par rapport à SAP WT. Ces résultats suggèrent une réponse immunitaire différentielle et des pressions de sélection virale chez les souris déficientes en SAP infectées par le SARS-CoV-2.

Acknowledgements

"The roots of education are bitter, but the fruit is sweet.", said Aristotle in Ancient Greece, more than 2000 years ago. To this date, in my point of view, this is quote remains valid every time students see the results of the hard work they put during their academic journey, be it short or long term.

During my masters, I have been very fortunate to have met and worked with incredibly supportive individuals who guided me, both academically and personally. Of those were my two dear mentors: Dr Silvia Vidal and Dr Levon Abrahamyan, both being instrumental in overseeing my development as a young scientist and fuelling my passion for the field of virology and virus-host interactions. I am incredibly grateful to both for believing in me and giving me the chance to work on a very interesting project that has played an important part in my life. My desire to contribute to the global effort against COVID-19, has been possible thanks to you. As Plutarch puts it: "The mind is not a vessel that needs filling, but wood that needs igniting".

Along with my mentors, I have had the pleasure to work with:

Dhanesh Patel, who showed me important lab skills and was always there to address my technical questions, even if there were repetitive at times. I thank you for all the help you've provided me and for the good times!

Patricia Caroline D'Arcy, who was crucial in helping with all *in vivo* experiments. Merci beaucoup pour ton aide! Je me souviendrai toujours des expériences de passage à 6-7h pendant la session d'automne 2022.

Dr. Mitra Yousefi, who was very important in training and supervising my work in the BSL3 lab; giving constructive advice and also helping with *in vivo* experiments. Thanks Mitra!

Benoît Charbonneau who was there to address any technical question I had before, during and after experiments. Merci beaucoup! Par contre, je n'ai pas assez d'argent pour te rembourser les 5$ à chaque fois que tu m'as aidé (hahaha).

Dr. Danielle Malo, for providing guidance as part of our platform, my supervisory committee, as well as helping in *in vivo* experiments. J'apprécie vraiment ton aide!

Dr. Gaël Galli, who provided me with a lot of guidance on the academic and personal level. Je te remercie énormément pour ton soutient, même à longue distance, tu m'as beaucoup aidé et motivé, surtout durant la première année, quand je venais tout juste de commencer – et les jours quand tout n'allait pas comme on voulait (avec les manips) :)

Dr. Catalina Barboza-Solís, who helped me with *in vitro*, and *in vivo* experiments. Estoy muy agradecido por toda la ayuda que me prestaste, especialmente en el BSL3. Fue un verdadero placer trabajar contigo, y pasamos unos días inolvidables con todo el equipo.

Alice Hou, who was crucial in helping me with mouse genotyping and was always there to give me a hand when at times, there were a lot on my plate. It was a pleasure for me to transmit my knowledge to you and help you during your masters. 谢谢你!

The team of Dr Jiannis Ragoussis including Ju-Ling Liu for providing me crucial help in sequencing our virus samples; and to Dr Julian Willett for analyzing the sequencing results. I greatly appreciate your help!

My other supervisory committee members: Dr Jörg Hermann Fritz and Dr Jesse Shapiro, for being so kind in guiding me throughout this project.

My lab members not previously mentioned: Jaren Abergas, Charlotte Fouquet, Alicia Reyes Valenzuela, Priya Nagpal, Anqi Yan and Mathieu Mancini. It was truly a pleasure working with all of you!

Friends and colleagues including Sai Sakktee Krisna, Dr. Angela Mingarelli, Nailya Ismailova, Audrey Roy-Dorval, Dania Shaban, Dr. Marija Landekic and everyone on the 3rd floor of the Bellini Building who helped me with questions and advice. Thank you very much!

Finally, my beloved parents who have always believed in me until today. I dedicate this thesis to you. Even in the hardest times, when all hope seemed lost, you stayed strong, and your experiences were crucial in inspiring me to endure throughout this journey, and in the next ones…

« Թէեւ մահուան շուքի ձորին մէջ ալ պտրտիմ, Չարէն պիտի չվախնամ,Վասն զի դուն ինծի հետ ես, Քու ցուպդ ու գաւազանդ՝ անոնք զիս պիտի մխիթարեն : » (Սաղմոս 23:4)

Author Contributions

Both Dr. Silvia Vidal and Dr. Levon Abrahamyan oversaw my work and mentored me during the entirety of my project. Dr Levon Abrahamyan showed me fundamental virology skills at his laboratory: cell culturing, viral propagation, and titration by $TCID_{50}$ assay. Dr. Silvia Vidal helped with experiments in the BSL3.

Dhanesh Patel taught me fundamental laboratory skills and showed me how to genotype, PCR, qPCR. He assisted me in viral titration, and sample processing in the BSL3.

Benoît Charbonneau helped planning experiments and assisted me in viral titration, and sample processing in the BSL3.

Dr. Mitra Yousefi helped plan and give advice for any experiment done in the BSL3. Patricia Caroline D'Arcy maintained all mouse colonies and with Dr Mitra Yousefi did the mouse infections and necropsies, alongside Dr. Danielle Malo and Dr. Catalina Barboza-Solís. Dr. Catalina Barboza-Solís also helped overseeing my BSL3 training and assisting with *in vitro* experiments.

Alice Hou helped with genotyping the mice and gave a hand in passing cells. Dr Gaël Galli assisted in experiment planning and gave a hand with sample processing.

Dr Ioannis Ragoussis' team helped sequencing our samples and Dr Julian Willett analyzed the sequenced data.

I sincerely thank you all for helping me complete this project!

My own contributions include all sample processing (i.e., RNA extraction), $TCID_{50}$ assays, genotyping mice, setting up animal experiments, qPCRs, and analysis of results.

List of Abbreviations

(h)ACE2: (human) Angiotensin converting enzyme 2

AAS: Amino acid substitution

ADCC: Antibody-dependent cellular cytotoxicity

B6: C57BL/6 mouse strain

BSL3: Biosafety level 3

COVID-19: Coronavirus disease 19

DMEM: (Gibco's) Dulbecco's Modified Eagle Medium

DMV: Double membrane vesicles

(c)DNA: (complementary) Deoxyribonucleic acid

DPI: Days post infection

EBV: Epstein-Barr virus

ER: Endoplasmic reticulum

ExoN: Exonuclease N

GAPDH: Glyceraldehyde-3-phosphate dehydrogenase

GZMB/*Gzmb:* Granzyme B

HLH: Haemophagocytic lymphohistiocytosis

HIV: Human immunodeficiency virus

IFN: Interferon

IFNγ/*Ifnγ*: Interferon gamma

K18: Epithelial cell cytokeratin-18

KO: Knock-out

LCMV: Lymphocytic choriomeningitis virus

MISC: Multisystem inflammatory syndrome in children

MHV68: Murine gammaherpesvirus 68

NCR: Natural cytotoxicity receptor

NET: Neutrophil extracellular traps

NK: Natural killer

NKT: Natural killer T

Nsp: Non-structural protein

NTD: N-terminal domain

ORF: Open reading frame

PBS: Phosphate buffer saline

PID: Primary immunodeficiency

(q)PCR: (quantitative) Polymerase chain reaction

PFU: Plaque forming units

PRF1/*Prf1:* Perforin 1

RBD: Receptor binding domain

RdRp: RNA-dependent RNA polymerase

RNA: Ribonucleic acid

RNA-seq: RNA sequencing

RTC: Replication-transcription complex

SAP: SLAM-Associated Protein

SARS-CoV-2: severe acute respiratory syndrome coronavirus 2

SH2: Src-homology 2

SID: Secondary immunodeficiency

SLAM: Signalling Lymphocytic Activation Molecule

$TCID_{50}$: Tissue culture infectious dose 50

TYK: Tyrosine kinase

VOC: Variant of concern

WHO: World Health Organization

WT: Wild type

XLP1: X-linked proliferative disease 1

List of Figures and Tables

Chapter I: Introduction & Review of the Literature

Clinical & Biological Context

With around 7 million deaths caused by SARS-CoV-2 infections[1] and the rapid emergence of the variants of concern (VOC), understanding the evolution of SARS-CoV-2 *in vivo*, and more specifically, identifying potential vulnerabilities of the virus during its replication within its host are of great importance. Co-evolution of viruses with their hosts is driven by genetic diversity that is selected through evolutionary pressures[2]. In fact, intra-host evolution of SARS-CoV-2 in immunodeficient patients, some of which are treated with antivirals or antibodies, may drive the emergence of variants[3-6]. Further, the signaling lymphocyte activation molecule (SLAM)-associated protein, SAP was first identified as the affected protein in cases of X-linked lymphoproliferative (XLP) syndrome characterized by a defective immune system[7]. SAP consists almost entirely of a single SH2 protein domain that interacts with the cytoplasmic tail of SLAM receptors[7,8]. Expression of these receptors is restricted to hematopoietic cells[9]. SAP-deficient mice recapitulate multiple immune defects of XLP patients, including impaired CD8+ and NK cell cytotoxicity, and the absence of circulating NKT cells[10-12]. NK cells comprise the first line of defense against virus infection[13] and CD8+ cells are part of the adaptive immune response with the role of killing infected cells[14]. Both of these cell types are affected during SARS-CoV-2 infection[13,14]. In addition, the mouse epithelial cell cytokeratin-18 K18-ACE2 transgenic model of SARS-CoV-2 infection replicates key features of COVID-19, including control of virus titer by day 7 post-infection, which is dependent on cell-mediated immunity[15].

Objective

Our overall objective is to understand the pressures exerted by the immune system in the intra-host evolution of SARS-CoV-2.

Hypothesis

We hypothesize that SAP-immunodeficiency, which is selective to immune cells of the initial anti-viral response, will result in a more severe phenotype of acute and chronic SARS-CoV-2 infection. To test hypothesis, we will first evaluate clinical, viral and cell makers of SARS-CoV-2 disease at early time-points after infection. Second, as surrogate of chronic infection, we will conduct serial passage of the virus for multiple periods outlasting 40 days of infection. We expect that these setting models intra-host SARS-CoV-2 evolution, that different mutation patterns will be observed in SAP WT and SAP KO mice, which would subsequently allow us to track mutations selected by SAP-associated mechanisms including NK cells and CD8 cells.

Comprehensive Literature Review

COVID-19 Pandemic and Disease

In the end of 2019, numerous cases of a new pneumonia-like disease were detected in Wuhan, Hubei Province, China[16]. It was soon after reported that the etiology of this disease was a novel coronavirus, known as SARS-CoV-2[17]. With time, the virus spread quickly around the world, resulting in the COVID-19 pandemic. As of June 11, 2023, cumulatively, 767,850,269 cases and 6,942,901 deaths have been reported[1]. Despite preventative health measures and the development of effective antiviral drugs and vaccines, VOCs, such as the ones from the omicron sub-lineage have emerged, with mutations in key viral genes, making them capable of escaping protection from

neutralizing antibodies in individuals previously infected and/or vaccinated[18,19]. As a result, the pandemic is still ongoing.

As a respiratory virus, SARS-CoV-2 causes COVID-19 disease, which can be classified based on the severity of symptoms[20]. As of March 6, 2023, there are 5 different categories of COVID-19 infection severities: (1) Asymptomatic or presymptomatic individuals test positively for SARS-CoV-2 antigen or nucleic acid, but do not experience any COVID-19 symptoms[20]. (2) Mild illness occurs in individuals who experience any of the various signs or symptoms of COVID-19 (i.e., fever, cough, sore throat, malaise, headache, muscle pain, nausea, vomiting, diarrhea, loss of taste and smell) but do not have shortness of breath, dyspnea, or abnormal chest imaging[20]. (3) Moderate illness occurs when individuals show evidence of lower respiratory disease, and their oxygen saturation (SpO_2) is ≥94% on room air at sea level[20]. (4) Severe illness can be characterized by SpO2 <94%, a ratio of arterial partial pressure of oxygen to fraction of inspired oxygen (PaO2/FiO2) <300 mm Hg, a respiratory rate >30 breaths/min, or lung infiltrates >50%[20].

(5) Critical illness refers to individuals who have respiratory failure, septic shock, and/or multiple organ dysfunction[20]. Before the availability of effective anti-SARS-CoV-2 vaccines, the strongest indicator of COVID-19 severity was advanced age, with the likelihood of mortality doubling every five years from childhood onward[21]. Now, unvaccinated males face a 1.5-fold higher risk of death compared to females[21]. Ancestry, social status, and various underlying medical conditions have been linked to increased disease severity and mortality rates, with odds ratios (OR) usually below 1.5 and rarely exceeding 2[21]. Human genetic predisposition also plays an important role, since 1 to 5% individuals suffering from life-threatening COVID-19 infections experience a deficiency in type II interferon production due to inborn errors of immunity (IEIs)[21]. Pre-existing neutralizing antibodies can also block type II IFN activity in approximately 15% of life-threatening cases[21]. In

addition, a subset of children develop a multisystem inflammatory condition, known as MISC associated with COVID-19, with gastrointestinal, rash and cardiovascular symptoms, and in severe cases, neurological symptoms, hepatitis and kidney injury[22]. Finally, in 10% of SARS-CoV-2 infections, a multisystemic debilitating illness known as long-COVID takes place which can impact several organ systems and can cause cardiovascular abnormalities, dysautonomia and myalgic encephalomyelitis/chronic fatigue syndrome, with no effective treatments available[23].

COVID-19 Pathogenesis –Immune Cells

There are a number of cell types that are central in COVID-19 pathogenesis, namely macrophages, monocytes and neutrophils, as well as innate and adaptive lymphocytes[24]. From the latter, mild disease has been shown to be characterized by the presence of macrophages with phagocytic, antigen-presenting and anti-inflammatory properties in the lung, in contrast to severe infections which leads to an accumulation of hyperinflammatory macrophages secreting proinflammatory chemokines and cytokines such as IL6, IL1β, IL8, CXCL10 and TNFα[24-26]. Upon release of the chemoattractant cytokines such as IL8, neutrophil influx to the lungs and it has been shown that the levels of the neutrophil-activating cytokine IL17 correlates with disease severity[24]. Increased levels of NET formation have been noted in COVID-19 patients, correlating with disease severity, especially in the lungs[27]. Additionally, neutrophils can also induce thrombosis in severe COVID-19 where NETs can trigger platelet activation[28].

NK cells are crucial cells against a variety of viral infections, in which NCRs such as NKG2D, and NKp46 can bind to viral proteins to induce antiviral responses[13,29,30]. These include apoptosis of infected cells by secretion of lytic molecules PRF1 and GZMB, release of proinflammatory cytokines with antiviral activity such as IFNγ and by eliminating virus-infected cells by ADCC[13]. In SARS-CoV-2 infection, NK cells have been shown to be able to recognize SARS-CoV-2 S

peptides via the NKG2D receptor and increase IFNγ production in *in vitro*[31]. It has been shown that blood CD56^{bright} NK cells are hyperactivated in COVID-19 patients, and express PRF1 and GZMB[32]. It has also been shown that Nsp13 of SARS-CoV-2 can form a complex with host-cell HLA-E and by doing so, impair binding with NKG2A, making target cells susceptible to attack by NK cells[33].

Moreover, in SARS-CoV-2 infections, SARS-CoV-2 specific CD8$^+$ T cells exhibit high levels of cytotoxic effector molecules such as IFNγ, GZMB, PRF1 and CD107a[14]. It has also been shown that SARS-CoV-2 mutations in MHC-I-restricted CD8$^+$ epitopes can evade CD8+ responses[34]. These suggest that both NK and CD8 cells are active in SARS-CoV-2 infection.

Replication Cycle of SARS-CoV-2 (adapted from Markarian & Galli et al 2023)[35]**:**

SARS-CoV-2 is a betacoronavirus that shares 96% of its genomic identity with the RaTG13 bat coronavirus and is hypothesized to be of zoonotic origin[36,37]. It is a positive sense ribonucleic acid virus (RNA), with a genome spanning around 30 kilobases in length[38,39]. Notably, two-thirds of its genome is composed of overlapping open reading frames (ORF) 1a and 1b, which together encode for an RNA-dependent RNA polymerase (RdRp) and other non-structural proteins important for viral replication and transcription[40-42]. The remainder of the viral genome is composed of ORFs 2–10 encoding for structural and accessory proteins[43-47].

Of the structural proteins, the spike is a large accessible homotrimeric protein of great importance in viral tropism and viral entry, making it an important target in therapeutic development[48]. With a molecular weight of around 180 kDa, the spike protein is composed of 2 major subunits per monomer: the S1 (residues 14–685) and S2 (residues 686–1273)[49,50]. The former is the most variable part of the spike among coronaviruses and contains the amino NTD and the receptor-RBD[49,50]. As for the S2, its domains, which are essential for viral fusion with the host cell

membrane, are more conserved in structure and sequence[49,50]. Besides the spike, there is the membrane protein, which is essential for viral assembly; the nucleocapsid, which plays a role in binding to the RNA genome of the virus ; and the envelope protein whose function is less known, and has been reported to interact with host proteins and act as a viroporin[51].

The main target of the spike protein is ACE2[52], a receptor that physiologically, plays an important role in the renin angiotensin system, a network involved in maintaining blood pressure, the level of electrolytes and homeostasis of fluids[53]. The broad expression of ACE2 explains in part SARS-CoV-2 pathogenesis in a multitude of organs from respiratory, circulatory, urogenital, gastrointestinal, and nervous systems[54]. From the latter, the most productive infection takes place in type I and II alveolar epithelial cells[24].

Following cell entry, the replication of SARS-CoV-2 takes place in the cytoplasm with the help of the host ribosomal machinery, translating the ORF 1a and 1b genes into two large replicase polyproteins, namely, pp1a and pp1ab[39]. Together, both pp1a and pp1ab polyproteins undergo proteolytic cleavage *via* the viral-encoded proteinases papain-like protease (PL-pro, Nsp3) and 3C-like protease (3CL-pro, Nsp5) to generate 16 mature non-structural proteins, i.e., Nsp1 to Nsp16[55]. Proteolysis is an essential step for viral replication, which is why antivirals targeting proteases are of interest[56,57]. Later, the RdRp (Nsp12), helicase (Nsp13), and Nsp7 to Nsp9 form the RTC, allowing the synthesis of both genomic and subgenomic viral RNA in DMVs at the periphery of the ER[58]. Among the subgenomic RNA produced, four of them give rise to structural proteins, which along with genomic RNA, are essential to assemble new virions and egressing the cell by lysosomal trafficking[59].

Mutations in Emerging Variants

As a nidovirus, SARS-CoV-2 encodes a unique proofreading enzyme 3′ to 5′ ExoN involved in excising faulty nucleotides inserted by RNA polymerases, thus ensuring replication fidelity[60,61]. Despite this proofreading mechanism, SARS-CoV-2 has shown a capacity to accumulate a wide range and high number of mutations[62]. A study of samples from the first wave and second wave of COVID-19 in Japan noted a mutation rate of $1.16–1.87 \times 10^{-3}$ base substitutions/site/year[63]. This is relatively low compared with the HIV subtype B, which can have a nucleotide substitution rate ranging from 5.25×10^{-3} to 1.60×10^{-2} substitutions/site/year in gag and env-gp120 genes[64]. However, there are more ways of generating genetic diversity including viral recombination, which is the generation of new progeny from two distinct strains of virus co-infecting a cell[65]. In the case of SARS-CoV-2, Pollett and colleagues performed a recombination analysis of a variety of coronaviral sequences including 100,000 SARS-CoV-2 sequences[66]. Through this analysis, they showed eight SARS-CoV-2 recombination events, two of them in the spike gene[66]. Earlier in 2021, a SARS-CoV-2 co-infection event of a single patient was reported with two strains with distinct lineages, which raises concern for the recombination of SARS-CoV-2 evolution[67].

Furthermore, the genetic variability of viruses is shaped through the selection pressure of their host cell or environment. The host has multiple immune defense mechanisms at cellular, tissue, and systemic levels that can interfere with viral replication and spread. An example of this is a study by Leist and colleagues, where a human-clinical isolate of SARS-CoV-2 was serially passaged six times in WT BALB/c mice, allowing the virus to acquire key mutations, leading to inflammatory responses and pneumonia in mice, previously not seen upon infection with the human-isolate virus[68]. Antiviral treatments that target specific viral proteins are another selective pressure that can result in the development of treatment-resistant mutants. For instance, a chronically infected

immunodeficient patient receiving remdesivir treatment resulted in a recurrent viral shedding, where there was an emergence of the E802D amino acid substitution in the RdRp of SARS-CoV-2, and this conferred a 6-fold increased resistance to remdesivir (based on ID_{50} values)[69].

Among SARS-CoV-2 infected individuals, patients with immunodeficiency, due to pre-existing health conditions, and those undergoing immunosuppressive treatment are particularly susceptible to SARS-CoV-2[3-6] . Many research groups have reported chronic infections and the accumulation of viral protein-coding mutations in such individuals in the presence of anti-COVID-19 treatments, with potential relevance at both biological and epidemiological levels[35,70,71]. The study of virus sequences that emerge in chronically infected patients could reveal regions of the virus genome that will be important as we prepare for future variants.

SAP Immunodeficiency and XLP1: insights from patients and mouse models

In the mid 1970s, Purtilo et al reported a novel X-linked disease in related individuals with a common ancestor named Duncan, where 6 out of 18 males died of a lymphoproliferative disease characterized by benign or malignant proliferation of lymphocytes triggered by EBV, histiocytosis and varying levels of serum immunoglobulins[72]. Soon after, it was determined that the X-linked lymphoproliferative disease 1 (XLP1) was caused by a loss-of function mutation in the *SH2D1A* gene on the long arm of the X chromosome (Xq25) which encodes the signalling lymphocyte activation molecule (SLAM)-associated protein (SAP). The *SH2D1A* gene in humans contains 4 exons, each of which has been reported to harbour mutations in XLP1 patients, among which exon 2 is the most commonly mutated[73]. SAP is expressed in NK, T and NKT cells, eosinophils, platelets and some B cells and is highly conserved across many species[74]. Structurally, SAP is a 128 amino acid cytoplasmic protein consisting of a central SH2 domain (98 amino acids), flanked by an NTD (5 amino acids), and CTD (25 amino acids)[75]. The main function of SAP is in cell transduction

and it does so by binding to phosphorylated ITSM motifs in the cytoplasmic tails of SLAM family receptors (with the exception of SLAMF2/CD48), which in turn, sterically interferes with SH2-containing phosphatases such as SHIP-1, SHP1 and SHP2[7,8]. Alternatively, SAP can form a ternary complex with SLAM and a Fyn tyrosine kinase, where the latter phosphorylates SLAM and results in an activation of downstream signalling pathways important for SLAM receptors[7,8]. Clinically, XLP1 patients have HLH (Haemophagocytic lymphohistiocytosis), which can lead to dysgammaglobulinemia and B cell lymphoma as well as others including aplastic anemia, vasculitis, chronic gastritis, and skin lesions[7,76]. HLH is an acute and rapidly progressive systemic inflammatory disorder with the common clinical manifestations of multiorgan failure, lymphadenopathy, hepatosplenomegaly and acute unremitting fever, and is characterized by hyperferritemia, cytokine storm syndrome and cytopenia[77]. Approximately 35% of XLP1 patients manifest symptoms without being infected with EBV, especially in EBV-negative young boys where HLH is observed[76], however, EBV-positive XLP1 patients tend to develop higher rates of dysgammaglobulinemia and lymphoma[76]. Although the mortality of this disease has been reduced from 75% to 29%, partly thanks to improved monitoring and supportive care, individuals with XLP1 remain susceptible to EBV[76].

Following the discovery of SAP, the study of SAP-deficient mouse models has resulted in better understanding the role of SAP in the immune system. Indeed, there have been reports of SAP-deficient mice with $CD4^+$ T cell dysfunction upon infection with LCMV, influenza and MHV68 and which leads to an impaired B cell proliferation, defective germinal center formation and antibody production[78-81]. Similar results have been reported in humans, where XLP1 patients were reported to have deficiencies in the number of memory B cells, $CD4^+$ T cells and found that SAP-deficient $CD4^+$ T cells where defective in providing help to B cells *in vitro*[82].

Additionally, it has been reported that NK cells are also impacted in SAP deficient mice, where the absence of SAP impaired activation of NK cells through the SLAM family receptor 2B4, in response to hematopoietic cells[83], and to an inhibition of NK cell-mediated cytotoxicity[84]. A defect in 2B4-receptor mediated NK cell cytotoxicity was also shown in XLP1 patients which led the authors to suggest that this could result in reduced cell lysis of EBV-infected B cells[85].

Moreover, acute infection with LCMV and MHV68 led to an increased number of virus-specific $CD8^+$ T cells and production of IFNγ by these cells in SAP deficient mice[10,86], which was shown to be associated with an impaired activation-induced cell death, due to a reduction of the mitochondrial T cell receptor-induced apoptosis mediator p73[11]. Another study also showed a $CD8^+$ T cell driven immunopathology in SAP deficient mice chronically infected with LCMV[87].

In humans, one study showed that EBV specific T cells generated from XLP1 patients showed a decrease in IFNγ production in response to 2B4 and EBV-transformed lymphoblastoid cell line stimulation[88]. In a subsequent study, it was revealed that there is a defective lytic activity of $CD8^+$ T cells specific to EBV-infected targets by failing to polarize 2B4, perforin and lipid raft marker GM1 at the contact with EBV-positive target cells[89].

Finally, upon stimulating SAP deficient mice with the NKT stimulus alpha-galactosyl ceramide, a complete lack of NKT cells in the thymus and peripheral organs has been reported[12,90,91], which agrees with findings in XLP1 patients, who also lacked NKT cells[12,91].

With these dysregulated immune responses in SAP deficiency, it of great interest of investigating the role of SAP in different pathogens, especially SARS-CoV-2. Although the prevalence of XLP1 occurs at a rate of 1-3 over 1,000,000 males[92], there are no case reports describing the effects of SARS-CoV-2 infection in patients with XLP1. However, it has been reported a rare case of fatal SARS with excessive and uncontrolled inflammation in a patient with XLP1[93]. During the

COVID-19 pandemic, another report showed an XLP1 patient, previously infected with SARS-CoV-2, succumbing to a fulminant HLH triggered by EBV. The contribution of SARS-CoV-2 on the EBV infection was unclear [94]. In order to better investigate the role of SAP in SARS-CoV-2 infections, one could use experimental animal models, such as mice, which as described earlier, have previously been used to study SAP deficiency in the context of LCMV, MHV68 and influenza infections. To also study the role of SAP in the context of SARS-CoV-2 infections, one could combine previously characterized SAP deficient mice with mouse models used to study COVID-19.

Mouse Models of COVID-19

Global efforts and contributions to fight against the COVID-19 pandemic allowed for advancements in research. One area in which this has been important is the development of COVID-19 mouse models. This was important since it had been found that mice bearing the murine ACE2 were not susceptible to early circulating strains of SARS-CoV-2[95]. Thus far, many research groups have developed new methods to make mice susceptible to SARS-CoV-2 infection. One way of doing so is by serially passaging clinical isolates in the respiratory tract of mice which has led to mouse-adapted SARS-CoV-2 strains that cause severe respiratory symptoms and mortality in WT mice[96-100]. Alternatively, the hACE2 receptor can be introduced into mice using (1) viral-vector transduction, (2) knock-in and (3) transgenic mice[101]. In the case of viral-vector transduction, the intranasal administration of replication-deficient adenoviruses or adeno-associated virus vector was able to transiently express hACE2 in lung tissues, and consequentially making mice permissive to SARS-CoV-2 infection and disease[102-104]. As for the hACE2 knock-in mice, hACE2 is expressed under an endogenous promoter of mACE2, where SARS-CoV-2 replication has been observed but without severe symptoms, making it a model of mild COVID-

19[105,106]. Lastly, the K18-hACE2 model is the most widely used COVID-19 mouse model due to its availability and use in previously studying SARS-CoV infection. This was achieved using the epithelial cell K18 gene promoter to drive the expression of hACE2, in the lung, trachea, kidney and brain of mice[107]. Upon infection with SARS-CoV-2, K18-hACE2 mice substantially lose weight up to 6 DPI at high or low doses[108], with increased viral titres noted in the lungs and nasal turbinates at 2 DPI,4 DPI and 7 DPI[15]. Recently, it has been shown that SARS-CoV-2 infection and replication through the brain leads to a loss of neurons, signs of glial activation and vascular damage[109]. In terms of immune correlates of protection, when infected with 25,000 PFU of SARS-CoV-2, the K18-hACE2 mice exhibit a significant increase of $CD45^+$ immune cells at 2 DPI in the BALF and 4 DPI in the lung tissue[15]. The cellular infiltrates at 4 and 7 DPI in the lung have been shown to mainly be composed of myeloid cell subsets including $Ly6G^+$ neutrophils, $Ly6C^+$ monocytes and $CD11b^+CD11c^+$ dendritic cells[15]. At 4 and 7 DPI, compared to the non-infected controls, an increase in various lymphoid cell subsets within the lung, including NK1.1+ NK cells, γδ $CD3^+$ T cells, $CD3^+CD4^+$ T cells, $CD3^+CD8^+$ T cells, and activated $CD44^+CD3^+CD8^+$ T cells were also observed[15]. A limitation in the K18-hACE2 mouse model is that expression of the hACE2 transgene is non-physiological as it is driven by the K18 promoter and can be expressed in tissues other than endogenously expressed ACE2; it is independent of regulatory mechanisms that control expression of hACE2; and 8 full copies are inserted in the mouse chromosome 2, despite being expressed on chromosome X in humans[15]. Despite these limitations, the K18-hACE2 has been very useful in studying the infectivity of different SARS-CoV-2 variants[110-112], testing vaccines[109,112-114], and antivirals[115-117] against SARS-CoV-2.

Chapter II: Materials & Methods

Mouse Breeding & Genotyping

C57BL/6 K18-hACE2 hemizygous transgenic mice were purchased from Jackson Laboratories (Bar Harbor, ME, USA), and mice with *SH2D1A* deficiency with a B6 background, were kindly provided by Dr. André Veillette (IRCM)[118]. Breeding was done to generate SAP knockout, hACE2 hemizygous (referred as SAP KO) and SAP wild-type, hACE2 hemizygous male mice (referred as SAP WT). All protocols were approved by the McGill University Animal Care Committee.

Genotyping

Ear punches obtained from mice were digested in DNA digestion buffer with Proteinase K for a minimum of 3 hours at 56°C and DNA was extracted by: addition of chloroform, extraction of aqueous phase, sequential addition and removal of isopropyl alcohol and alcohol, and finally pellet drying[119]. PCR reactions were then run on a 1% agarose gel containing ethidium bromide in TBE buffer in gel chambers. Bands were visualized on the Molecular Imager® Gel Doc TM XR system (Bio-Rad).

SAP Genotyping

PCRs were run using the primer pair specific for SAP (*SH2D1A* gene) (**Supplementary Table 1**). The PCR amplification protocol was: 95°C for 3 minutes, 30 cycles of 95°C for 25 sec, 57.5°C for 25 sec, 72°C for 45 sec followed by a cycle at 72°C for 5 min. A single band of 400 bp in size observed by gel electrophoresis signified that the mouse was either hemizygous (for males) or homozygous for the SAP mutant allele (in both male and females). Three bands, at 400 bp, 800 bp and 1083 bp, were observed if the mouse was heterozygous (in the case of females only). A single band of 1083 bp in size observed in gel signified that the mouse was WT for the SAP mutant allele (in both males and females).

hACE2 Genotyping

PCRs were run using the primer pair specific for duplicated region of Chr 2 linked to the (K18-ACE2)2Prlmn transgene (**Supplementary Table 1**)[120].

The PCR amplification protocol was: 95°C for 3 min, 35 cycles of 95°C for 15 sec, 55°C for 15 sec, 72°C for 15 sec followed by a cycle at 72°C for 1 min. Following the PCR reaction, the HpyCH4V restriction enzyme (New England Biolabs) was added to cut at an SNP created when generating the tg(K18-ACE2)2Prlmn transgene. The digestion run: 37°C for 40 min, 65°C for 20 min.

A single band of 285 bp in size observed in gel indicated a WT genotype for hACE2. Two bands (often seen as one) of 148 bp and 137 bp indicated a homozygous genotype for hACE2. Three bands (often seen as two bands) at 285 bp, 148 bp and 137 bp indicated a hemizygous genotype for hACE2, which are selected for infection[120].

A representative picture of SAP and hACE2 genotyping are shown in **Supplementary Figure 1.**

Viral Stock Production

The McGill University Health Center provided a clinical viral isolate called SARS-CoV-2 CP13.32 (Genbank accession no. 599736; lineage B1.1.147), which had been isolated before November 2020. This stock was propagated as previously described[121]. A list of amino acid changes and mutations in this viral stock relative to the original Wuhan-Hu-1 NC_045512 sequence are presented in **Supplementary Table 2**.

Mouse Infections

Acute infection experiments

Infections were carried out in the BSL3 laboratory at McGill University. Male SAP KO and WT mice were first anesthetized with isoflurane, and then intranasally challenged with either 50 PFU

(low dose), 5000 PFU (medium dose) or 25000 PFU (high dose) of SARS-CoV-2, in an inoculum of 20 uL per mouse. Clinical signs were monitored following the clinical scoring system shown in the **Supplementary Table 3** of the Results section. The mice were monitored twice daily starting from day 4, for low dose, and day 3, for medium and high dose, mice were monitored twice daily. For infections conducted with low and medium dose, two separate survival experiments were performed. In the first low dose experiment, 5 SAP KO and 5 SAP WT male mice were infected, lung and brain tissue (frontal lobe) were recovered from mice at the different days of euthanasia for $TCID_{50}$ assay and qPCR (for both lung and brain samples) and histology analysis (for collected lung samples). In the second low dose experiment, 9 SAP KO and 8 SAP WT were infected, and clinical signs, BW loss were monitored. The clinical results (survival, clinical scores, BW loss) from the first and second low dose experiment were pooled together and shown in the Results section **(Figure 1)**.

Two survival experiments were also done with female mice infected with a low dose (total of 9 SAP KO and 8 SAP WT).

In the first medium dose experiment, 7 SAP KO and 4 SAP WT were infected, lung and brain tissue (frontal lobe) were collected at 5 DPI for $TCID_{50}$ assay and qPCR. In the second medium dose experiment 5 SAP KO and 5 SAP WT mice were infected where lung tissue and serum were collected at 5 DPI for $TCID_{50}$ assay, qPCR, histology and cytokine protein level multiplex analysis.

In the high dose experiment, 4 SAP KO and 5 SAP WT mice were infected, and lung tissue and the BALF were collected at 5 DPI. Lung tissue was used for $TCID_{50}$ assay and qPCR; while the BALF was used for cytokine protein level multiplex analysis.

Serial passaging of SARS-CoV-2

For serial passaging experiments, a dose of 7.0 x 10^5 PFU per mouse (in 25 uL inoculum) of CP13.32 P4 passage 5 (P0) was used to infect 3 SAP KO and 3 SAP WT mice; at 4 DPI, the mice underwent necropsy to recover entire lungs, which were homogenized and clarified twice (remove supernatant and spin at 12,000xg for 15 min at 4 °C), aliquoted and frozen at -80°C. In the subsequent passages, the clarified lung homogenates of the previous passages were thawed, clarified again (remove supernatant and spin at 12,000xg for 3 min at 4 °C) and used to infect mice of the same genotype, thus creating 3 separate passaging lineages per mouse genotype. For each sample the remaining aliquots per passage were used for viral titration, purification, and viral RNA sequencing.

Infectious Virus Titrations

The TCID50 method was adapted from Amarilla et al (2021)[122]. A day before infection, approximately 2.50 x 10^4 VeroE6 cells (ATCC, #CRL-1586) per well were seeded in a 96-well plate and incubated overnight to reach 100% confluency. The day of infection, the VeroE6 cell medium was changed to plain DMEM media during transport to the BSL3 facility; In the BSL3, clarified lung homogenate samples were thawed and ten-fold serially diluted in plain DMEM from 10^{-1} to 10^{-8}. Media was removed and 100uL each viral dilution was added per well, five replicates per dilution. Cells were incubated at 37 °C for 72 h and at 3DPI, the CPE was scored using a light microscope. Fifty percent endpoints were calculated using Reed and Muench's (1938)[123] calculation and expressed as tissue culture infectious dose ($TCID_{50}$)/mL.

RNA Extraction & qPCR

The collected and sectioned lung samples were added to RNAlater™ (Invitrogen, # AM7021) and kept at 4 °C for 48 h, before being transferred at -20 °C. Tissues were then thawed, added to 1 mL TRIzol reagent (Invitrogen, #15596018), homogenized and clarified twice. RNA was extracted using the PureLink RNA Mini Kit (Invitrogen, #2535444A), following the manufacturer's protocols. Samples then underwent DNase I (Sigma, #4716728001) treatment at a cycle of 37 °C for 15 min and 95 °C for 10 min and the isolated RNA was reverse transcribed using the High-Capacity cDNA Reverse Transcription Kit (Applied Biosystems, #368814). The 8-fold diluted cDNA was amplified in presence of primers and *Power* SyBr Green PCR Mix (Applied Biosystems, #4367659) at a cycle 95 °C for 10 min followed by 40 cycles of 95 °C for 10 sec, 60 °C for 20 sec, and 70 °C for 15 sec. The sequences of primer pairs used are shown in **Supplementary Table 1**.

Viral RNA Sequencing, Data Processing and Analysis

Viral RNA sequencing and processing was performed as reported previously[124]. In summary, RNA extracted from P0 virus stock, P4 and P10 SAP KO and SAP WT clarified lung homogenates (n=3 per genotype, per passage) underwent reverse transcription and targeted SARS-CoV-2 amplification using the ARTIC V4.1 primer scheme. The resulting samples were then purified, and Nextera DNA Flex library preparation was carried out for Illumina PE150 paired-end amplicon sequencing using best practices on a NovaSeq instrument at the McGill Genome Centre (Montreal, QC, CA). Following sequencing, the resulting alignments for each sample were sorted with duplicate reads flagged, and the minimum number of aligned reads for each was recorded. Each sample was then re-aligned and processed, and randomly down sampled to match this minimum number of reads. Freebayes v1.3.6 was used to call variants from these reads, and the

results were saved as a VCF file. Any variant alleles with a quality of less than 20 or a depth below 10 were excluded from the analysis. In addition, any variant alleles that overlapped with ARTIC sequencing primers were also removed. This curated output was used to compare genomic variation across passages.

Plasma/BALF Cytokine Analysis

Cardiac puncture was performed on isoflurane-anaesthetized mice to obtain blood. Plasma was obtained by addition to ethylenediaminetetraacetic acid tubes and spun at 3000xg for 10 min at room temperature. BALF was obtained by tracheal intubation, inflation of the airways with 0.5 mL PBS for four times and collection of the fluid. BAL fluids were centrifuged at 800xg at 4°C for 10 min. Both the plasma and BALF were virus-inactivated by addition of 1% Triton X-100 and left for 1 h at room temperature before immediately being frozen at -20°C. Samples were shipped to Eve Technologies (Calgary, AB, CA) for the Mouse Cytokine Proinflammatory Focused 10-Plex Discovery Assay® Array (MDF10).

Histology Analysis

According to the SOP, half of the mouse lungs were collected in cassettes and fixed in 10% PFA for 7 days before exiting the CL3 facility. The samples were whole mounted on glass slides and stained with hematoxylin and eosin with the help of the Histology Core Facility at the McGill Goodman Cancer Institute (Montreal, QC, CA). The slides were analyzed at the TCP Pathology Core at The Centre for Phenogenomics (Toronto, ON, CA) by a certified pathologist (Dr. Mohammad R. Eskandarian, University of Toronto).

Statistical methods

All statistics were calculated using GraphPad Prism version 9 for Mac (GraphPad Software, San Diego, California, USA). Due to small numbers and data that are possibly not normally distributed, the nonparametric Mann-Whitney test was used to compare different groups of mice (e.g. KO

infected and WT infected). When comparing four groups (KO and WT infected and uninfected respectively), the Kruskal-Wallis test was used, with Dunn's multiple comparison test. A p-value ≤ 0.05 was considered significant.

Chapter III: Results

(i) No clinical differences observed between infected SAP KO and WT

In this study, the first objective was to compare the dynamics of SARS-CoV-2 infection SAP KO with K18-hACE2 hemizygous mice (SAP WT). It was hypothesized that SAP WT mice would have a less severe phenotype in response to SARS-CoV-2 infection, compared to SAP KO mice, ultimately resulting in a different immune response. Comparing the survival of SAP KO and WT mice infected at 50 PFU (low dose), no notable difference can be observed for both the male **(Figure 1)** and female **(Supplementary Figure 2)** cohorts, which allowed us to continue our studies in male mice. Looking at male mice, the low dose infected ones succumbed between 6 DPI and 9 DPI for both SAP KO and WT cohorts. This similarity is also maintained at higher doses, succumbing between 5 DPI and 6 DPI for 5000 PFU infected mice **(Figure 1)**; and at 5 DPI for 25000 PFU infected mice (not shown). Looking at the clinical signs, which includes monitoring body weight, ruffled fur, hunching, mobility, dyspnea, no differences in BW loss for both SAP KO and WT at 50 PFU, 5000 PFU and 25000 PFU **(Figure 1)**. Lung histology, studied by hematoxylin and eosin (H&E) staining, showed an interstitial pneumonitis with heterogeneous alveolar walls thickening was noted for SAP KO and WT infected with low and medium doses at 6 DPI and 5 DPI respectively (**Supplementary Figure 3**). An intra-alveolar edema and interstitial widening with exudative diffuse hyaline membranes was observed with patchy intra-alveolar plugs of fibrin and interstitial inflammation, with mixed inflammatory cells that were present, but without fibrosis or organizing/proliferative appearance (**Supplementary Figure 3**). However, no difference in pathology was noted between SAP KO and WT infected mice **(Supplementary Figure 3)**. These results show that the time of appearance of disease symptoms and time of death

correlate with the infectious dose and that that there is no difference in infection between SAP KO and WT at the clinical level.

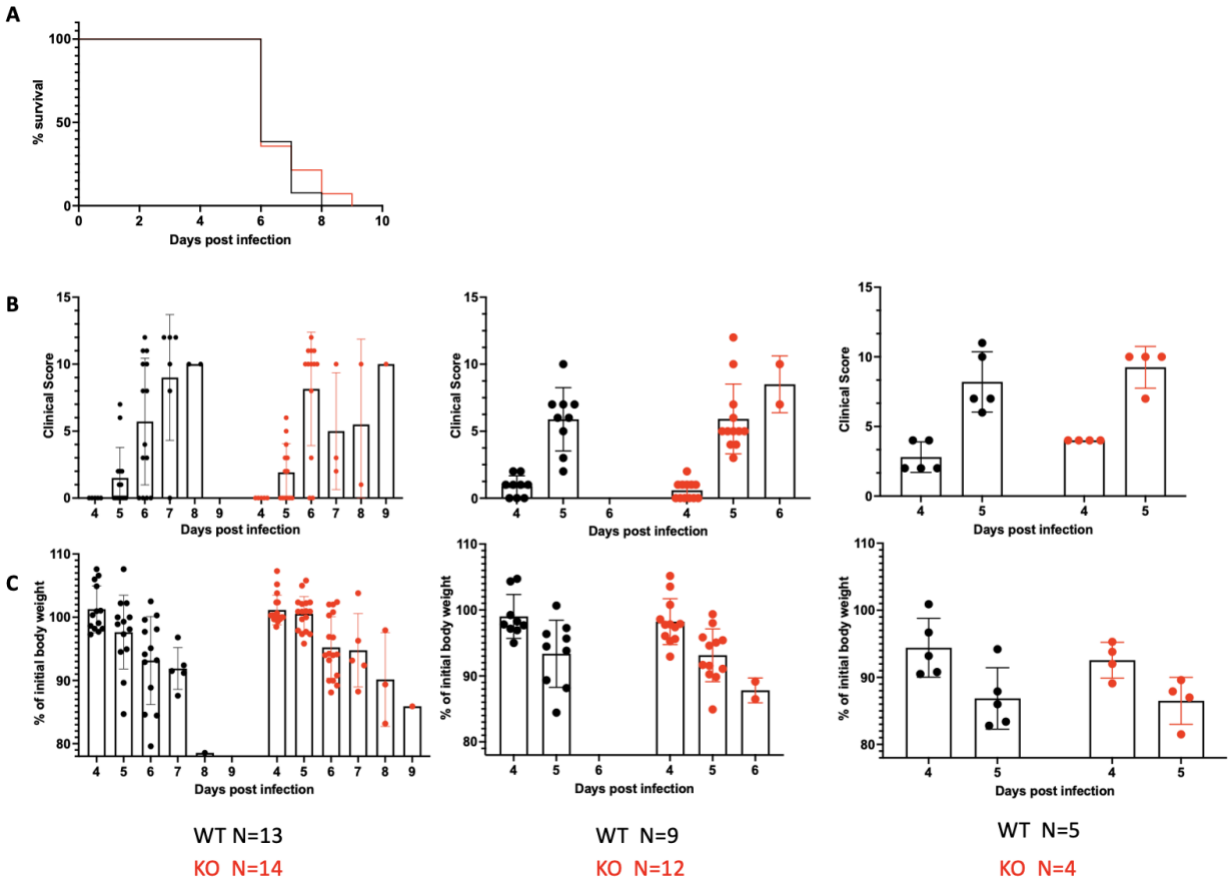

Figure 1: No difference in survival and body weight loss between SAP KO and WT male mice. **(A)** Percent survival relative to day 0 (100%) measurements are shown for mice were infected with low dose (SAP KO n=14; WT n=13). **(B)** Clinical scores for low, medium and high dose infected mice (left to right). **(C)** Percent body weight loss relative to day 0 (100%) for mice infected low dose (SAP KO n=14; WT n=13), medium dose (SAP KO n=12; WT n=9) and high dose (SAP KO n=4; WT n=5) is presented as the mean. The red dots represent SAP KO mice and the black dots represent SAP WT.

(ii) No differences in viral load observed between infected SAP KO and WT

In order to determine the viral load in our studied mice, this was done by looking at infectious viral titres (TCID50) and at viral RNA (qPCR).

The viral load in the lungs were next investigated at 6 DPI for mice infected at 50 PFU and at 5 DPI for mice infected with 5000 and 25000 PFU. For mice infected with 50 PFU, a titre of $1.98\times10^5 \pm 1.41\times10^5$ TCID50/g for the SAP WT and $3.48\times10^5 \pm 2.08\times10^5$ TCID50/g for the SAP KO **(Figure 2)**. For mice infected with 5000PFU, a titre of $7.70\times10^5 \pm 5.45\times10^5$ TCID50/g for the SAP WT and $3.33\times10^5 \pm 2.74\times10^5$ TCID50/g for the SAP KO **(Figure 2)**. For mice infected with 25000 PFU, a titre of $2.69\times10^5 \pm 2.04\times10^5$ TCID50/g for the SAP WT and $3.69\times10^5 \pm 1.67\times10^5$ TCID50/g for the SAP KO **(Figure 2)**.

In addition, the viral titre determined in the frontal lobe of the brain of mice was determined to be $4.21\times10^8 \pm 1.14\times10^8$ TCID50/g and $3.03\times10^8 \pm 5.84\times10^7$ TCID50/g at 6 DPI for SAP WT and KO mice infected with 50 PFU respectively **(Supplementary Figure 4)**. For mice infected with 5000 PFU, at 5 DPI, the viral titre in the frontal lobe of the brain was $4.11\times10^8 \pm 4.00\times10^8$ TCID50/g and $4.67\times10^7 \pm 3.48\times10^7$ for SAP WT and KO respectively. Although a higher viral titre was found in the brain compared to the lungs, there was no notable difference between SAP KO and WT.

Looking at the viral gene expression in the lungs of mice, there was $3.02\times10^3 \pm 9.01\times10^2$ SARS-CoV-2 S gene expression relative to *Gapdh* for the SAP WT compared to $3.17\times10^3 \pm 9.49\times10^2$ for SAP KO infected at 6 DPI after infection with 50 PFU **(Figure 2)**. For 5000 PFU infected mice, at 5 DPI, a relative S gene expression of $1.64\times10^3 \pm 5.27\times10^2$ and $3.34\times10^3 \pm 1.03\times10^3$ was observed for SAP WT and SAP KO respectively **(Figure 2)**. For 25000 PFU infected mice, at 5

DPI, a relative S gene expression of $8.43\times10^{3} \pm 2.64\times10^{3}$ and $1.10\times10^{4} \pm 4.56\times10^{3}$ was observed for SAP WT and SAP KO respectively **(Figure 2)**. With these results, it can be said that there is no difference infectious viral titre and expression of S gene between SAP WT and SAP KO upon infection with SARS-CoV-2, and that the disease severity is independent of viral load in the K18-hACE2 model.

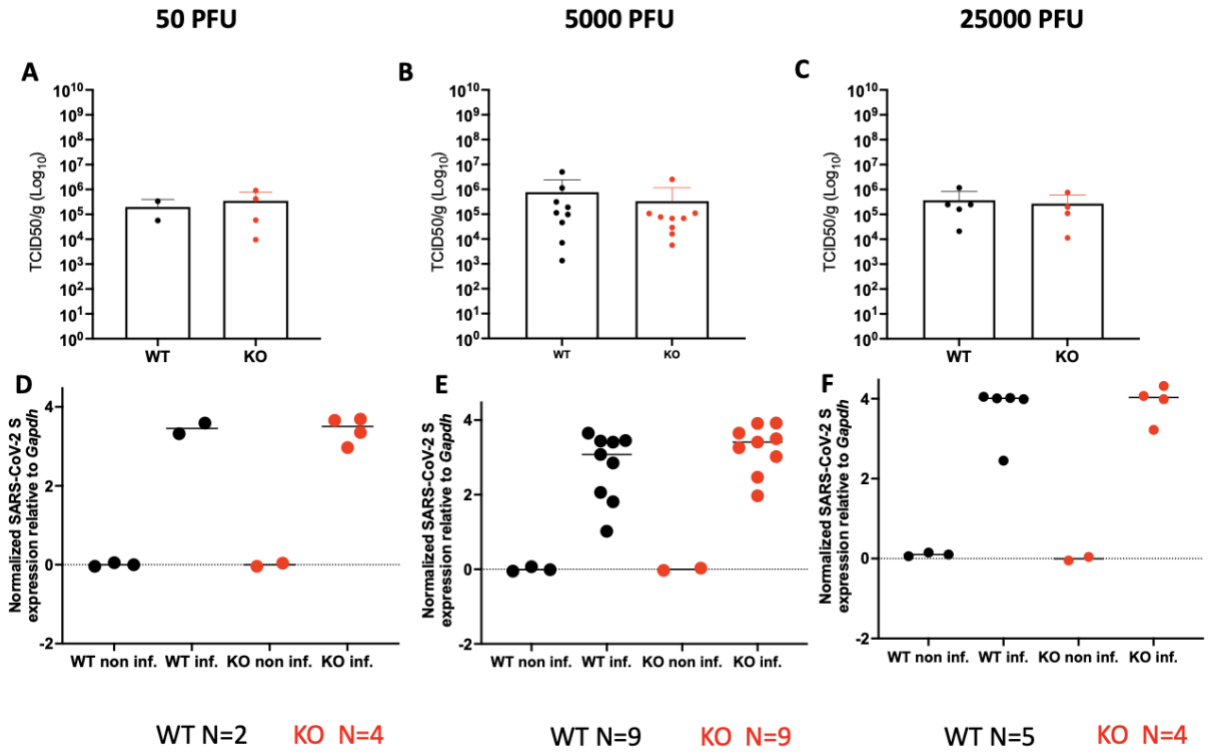

Figure 2: No difference in viral markers between SAP KO and WT male mice. Infectious viral titres reported as log (TCID50 per gram of lung) for mice infected at **(A)** 50 PFU (SAP KO n=14; WT n=13), **(B)** 5000 PFU (SAP KO n=12; WT n=9) and **(C)** at 25000 PFU (SAP KO n=4; WT n=5). Relative expression of SARS-CoV-2 S gene reported as log(delta-delta cycle threshold (ddCt)) and these were normalized to *Gapdh*, and to uninfected control groups, for mice infected with **(D)** 50 PFU, **(E)** 5000 PFU and **(F)** 25000 PFU of SARS-CoV-2. The red dots represent SAP

KO mice and the black dots represent SAP WT, and the horizontal bars indicate the mean per group.

(iii) Increased Expression of Molecular Immune Markers in SAP KO vs WT

With no differences observed in the clinical and virological phenotypes between SAP KO and WT mice upon infection, we then investigated the effects of SARS-CoV-2 on the expression of immune genes in SAP KO and WT mice. Since SAP deficient mice are known to have defects in NK cell cytotoxicity, and hyperproliferating $CD8^+$ cells upon infection, we chose to investigate the expression of the NK cell specific *Nkp46* gene[125], the *CD8α* gene expressed by $CD8^+$ cells[126], as well the expression of their cytotoxic effector genes *Ifnγ, Gzmb, Prf1*. This approach was taken as a surrogate of monitoring different cell types, as was done waiting for alternative approaches to monitor the cell response (i.e., flow cytometry).

The qPCR data showed no differences for *Nkp46* relative expression compared to *Gapdh* at all doses examined **(Figure 3)**. In contrast, there was a trend toward *CD8α* gene expression relative to *Gapdh* in the SAP KO infected mice compared to the SAP WT at low and medium dose **(Figure 3)**. For the low inoculum dose, the fold change of *CD8α* was 0.53 ± 0.28 for the SAP WT, which was lower than the 2.25 ± 0.99 fold change in the SAP KO **(Figure 3)**. Similarly, as for the medium dose, the SAP WT had *CD8α* fold change of 1.14 ± 0.29, which was lower than the SAP KO which had a fold change of 10.90 ± 4.53 **(Figure 3)**. As for the high dose infected mice, a significant increase of *CD8α* relative expression compared to *Gapdh* was noted in the SAP KO (fold change 2.64 ± 0.68) compared to the SAP WT (fold change of 0.57 ± 0.09).

As for *Ifnγ* expression vs *Gapdh*, although not significant, a trend for an increase was observed at all doses **(Figure 3)**. At low dose, SAP WT mice had a fold change of 24.40 ± 23.70 while the

SAP KO had 72.00 ± 19.80; at medium dose, SAP WT mice had a fold change of 34.02 ± 11.94 while the SAP KO had 65.65 ± 30.8; at high dose, SAP WT mice had a fold change of 28.81 ± 15.65 and the SAP KO had a fold change of 156.44 ± 40.02 **(Figure 3)**. Interestingly, the increased trend of *Ifnγ* expression in SAP KO was also noted in the plasma of medium dose infected mice; as well as in the BALF of high dose infected mice **(Supplementary Figure 5)**. Looking at the NK and $CD8^+$ specific cytotoxic molecule genes *Gzmb* and *Prf1*, similar trends of elevation in infected SAP KO compared to SAP WT were observed when looking at the relative gene expression vs *Gapdh* **(Figure 3)**. Low dose infected SAP WT mice had a fold change of 0.43 ± 0.04 for *Gzmb* and 0.11 ± 0.05 for *Prf1*, whereas the SAP KO had a higher fold change of 3.55± 2.16 for *Gzmb* and 0.72 ± 0.08 for *Prf1* **(Figure 3)**. As for the medium dose infected SAP WT mice, a fold change of 3.20 ± 2.74 for *Gzmb* and 0.83 ± 0.16 for *Prf1* was found, whereas the SAP KO had a similar fold change of 3.78 ± 1.74 for *Gzmb* and a higher 2.03 ± 0.64 for *Prf1* **(Figure 3)**. Finally, at the high dose infected SAP WT mice, a fold change of 1.13 ± 0.91 for *Gzmb* and 0.66 ± 0.20 for *Prf1* was observed, whereas the SAP KO had a significantly higher fold change of 9.91 ± 2.05 for *Gzmb* and 1.83 ± 0.36 for *Prf1* **(Figure 3)**.

All in all, these results show that there is a significantly higher expression of *CD8α*, *Gzmb* and *Prf1* in the lungs SAP KO infected mice compared to SAP WT mice at a higher dose and an upward trend at lower doses (low and medium). A trend to higher expression of *Ifnγ* was also observed at all doses in the SAP KO compared to SAP WT infected mice. Whether this is the case at the cellular level should be investigated in further studies.

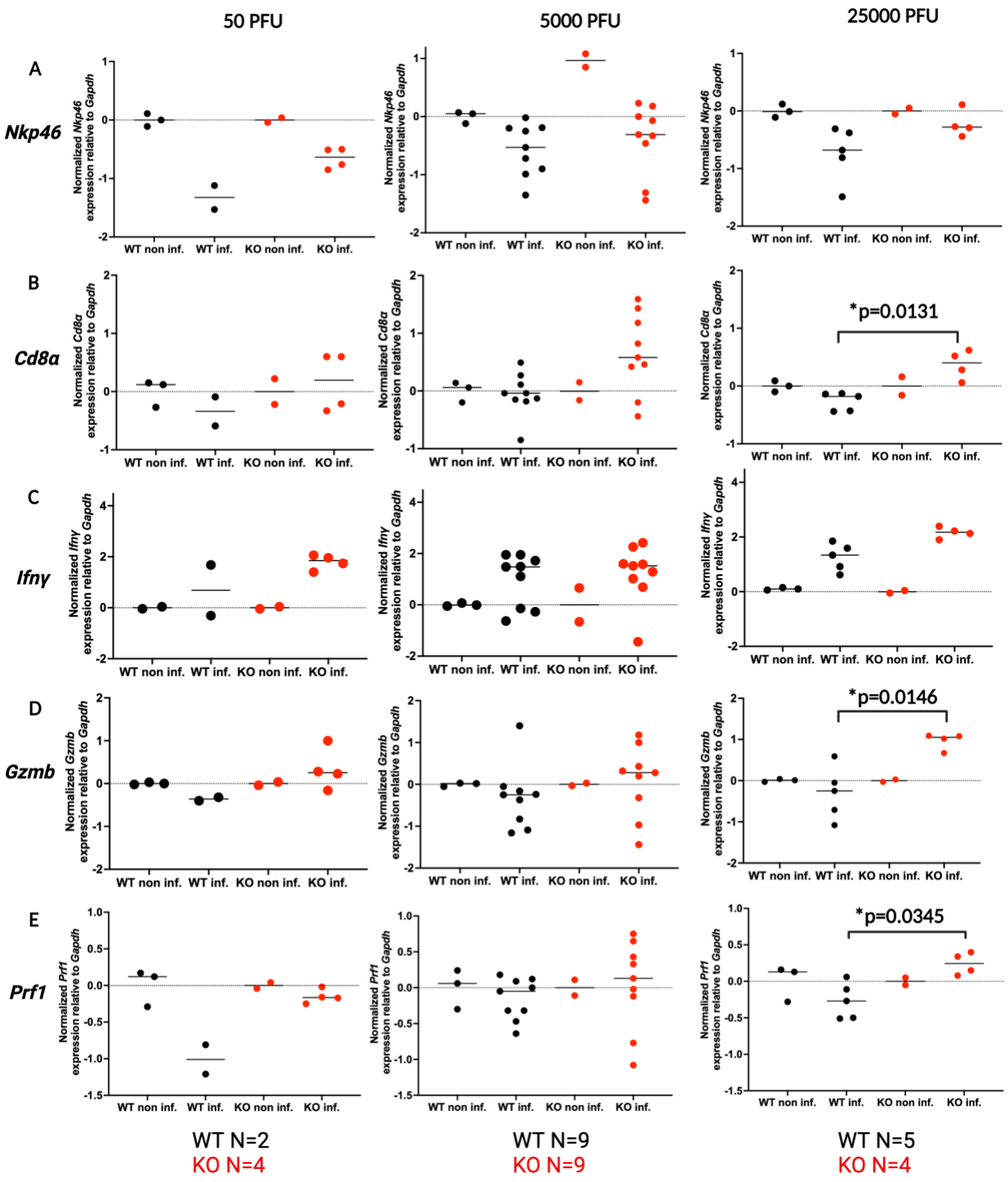

Figure 3: Increased Expression of Molecular Immune Markers in lungs of SAP KO vs WT male mice. Relative expression of **(A)** *Nkp46*, **(B)** *Cd8α*, **(C)** *Ifnγ*, **(D)** *Gzmb*, **(E)** *Prf1* genes reported as log(delta-delta cycle threshold (ddCt)) and these were normalized to *Gapdh*, and to uninfected

control groups, for mice infected with low (50 PFU), medium (5000 PFU), and high (25000 PFU) of SARS-CoV-2, from left to right respectively. The red dots are indicative of SAP KO mice and the black dots of SAP WT, and the data is presented as the mean per group. p*<0.05, SAP KO infected to SAP WT infected.

(iv) No difference in clinical and viral markers in serial passaged viruses in SAP KO vs SAP WT

With differences in the expression of immune genes in SAP KO mice vs SAP WT upon infection with SARS-CoV-2, we next performed serial passages of lung homogenates taken at 4 DPI in SAP KO and WT, generating 3 distinct lineages of viruses per genotype. Looking at the clinical scores, BW loss, viral titres and initial viral inoculi in these lineages at each passage at 4 DPI, no significant difference was noted **(Figure 4)**. However, on P5, the SAP KO mice had a trend towards higher clinical scores and BW loss compared to the SAP WT. These results are summarized in **Figure 4**.

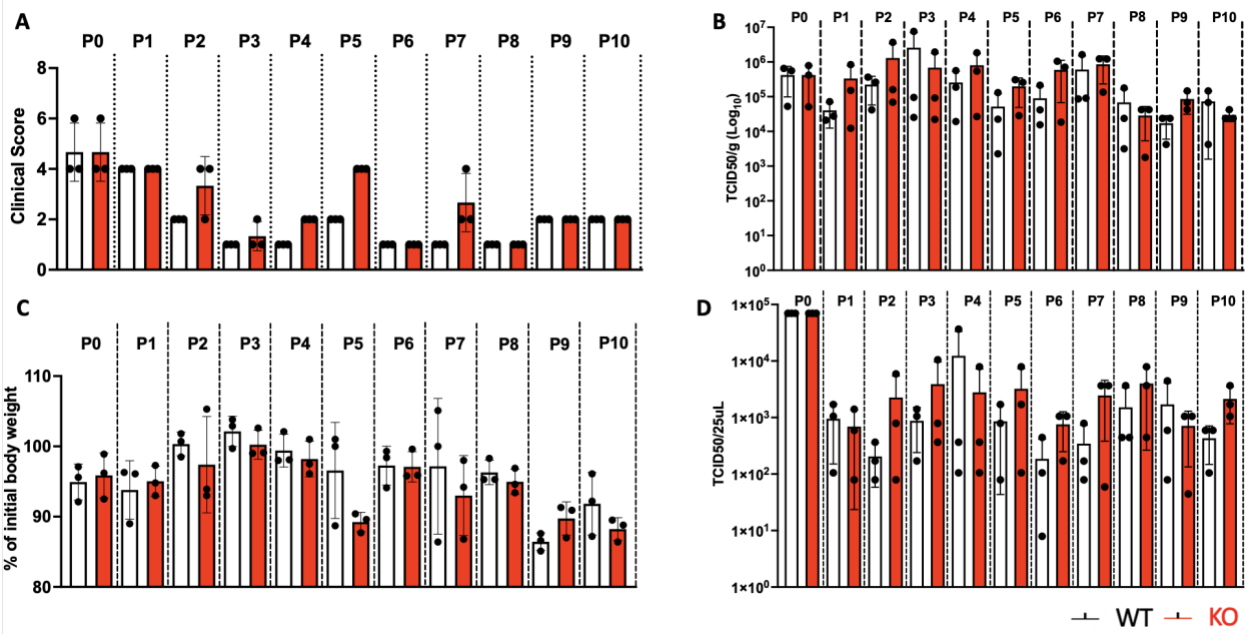

Figure 4: No difference in clinical and viral markers in serial passaged viruses in SAP KO vs SAP WT male mice. **(A)** clinical scores, **(B)** infectious viral titre in lung tissue, **(C)** BW loss and **(D)** and initial inoculum across different viral passages between SAP KO (red columns) and WT (white columns) at 4 DPI.

(v) Differential mutational profiles between SAP KO and SAP WT passaged viruses

To analyze the mutational profile of viruses passaged in SAP KO and WT mice,

the original viral stock used for passaging (P0), the lung homogenates of different lineages from P4, used as the inoculi for P5, as well as the last passage lung homogenates (P10), we performed RNA sequencing for analysis. Novel mutations compared to the P0 stock were found in both SAP KO and SAP WT passaged viruses, at P4 and P10, with a minor allele frequency greater or equal to 0.5. In SAP KO and SAP WT viral lineages, mutations occurred in the ORF1ab, Spike and Nucleocapsid genes (**Figure 5A, 5B)**. When summing up the total number of novel mutations the same passage and mouse genotype, we observed a trend towards a higher number of mutations in

the SAP KO passaged viruses for P4 (n=24) and P10 (n=27), compared to the SAP WT passaged viruses at P4 (n=19) and P10 (n=17) **(Figure 5A, 5B, 5C)**. Mutations were present in spike, nucleocapsid and ORF1ab, however the gene harbouring the most changes in SAP KO passaged viruses was the spike with an aggregated 9 mutations for the P4 and 11 for P10, in comparison with 5 and 4 mutations for the P4 and P10 viruses passaged in SAP WT mice **(Figure 5D)**. Furthermore, some mutations were specifically detected in SAP KO passaged viruses such as the spike A22206G (AAS D215G), nucleocapsid G28875T (AAS S201I), ORF1ab C4540T. In addition, the spike A22296G mutation (AAS H245R) was detected in all viruses passaged *in vivo* but was not detected in the P0 stock. Furthermore, two mutations in the spike: T21784A (AAS N74K) and G23607A (AAS R682Q) detected in the stock P0 were not detected in *in vivo* passaged viruses. Finally, some mutations arose in P4 for both SAP KO and WT passaged viruses however were either not detected or were reduced in the number of SAP WT passaged lineages with the mutation at P10. This is the case of the ORF1ab A4420G mutation detected in 2/3 SAP WT passage lineages and 3/3 SAP KO passage lineages at P4; 1/3 for SAP WT and 3/3 for SAP KO lineages at P10. Another mutation was the spike C23525T (AAS H655Y) detected in 2/3 SAP WT and SAP KO passage lineages at P4; not detected for SAP WT lineages and 2/3 for SAP KO lineages at P10. Finally, the T28843G (AAS S190R) mutation in the nucleocapsid gene was detected in 2/3 SAP WT and 3/3 SAP KO passage lineages at P4 but not detected for SAP WT lineages and 3/3 for SAP KO lineages at P10. These mutations of interest are shown in **Figure 5E**. These results indicate a differential mutational profile in SAP KO passaged viruses compared to SAP WT ones.

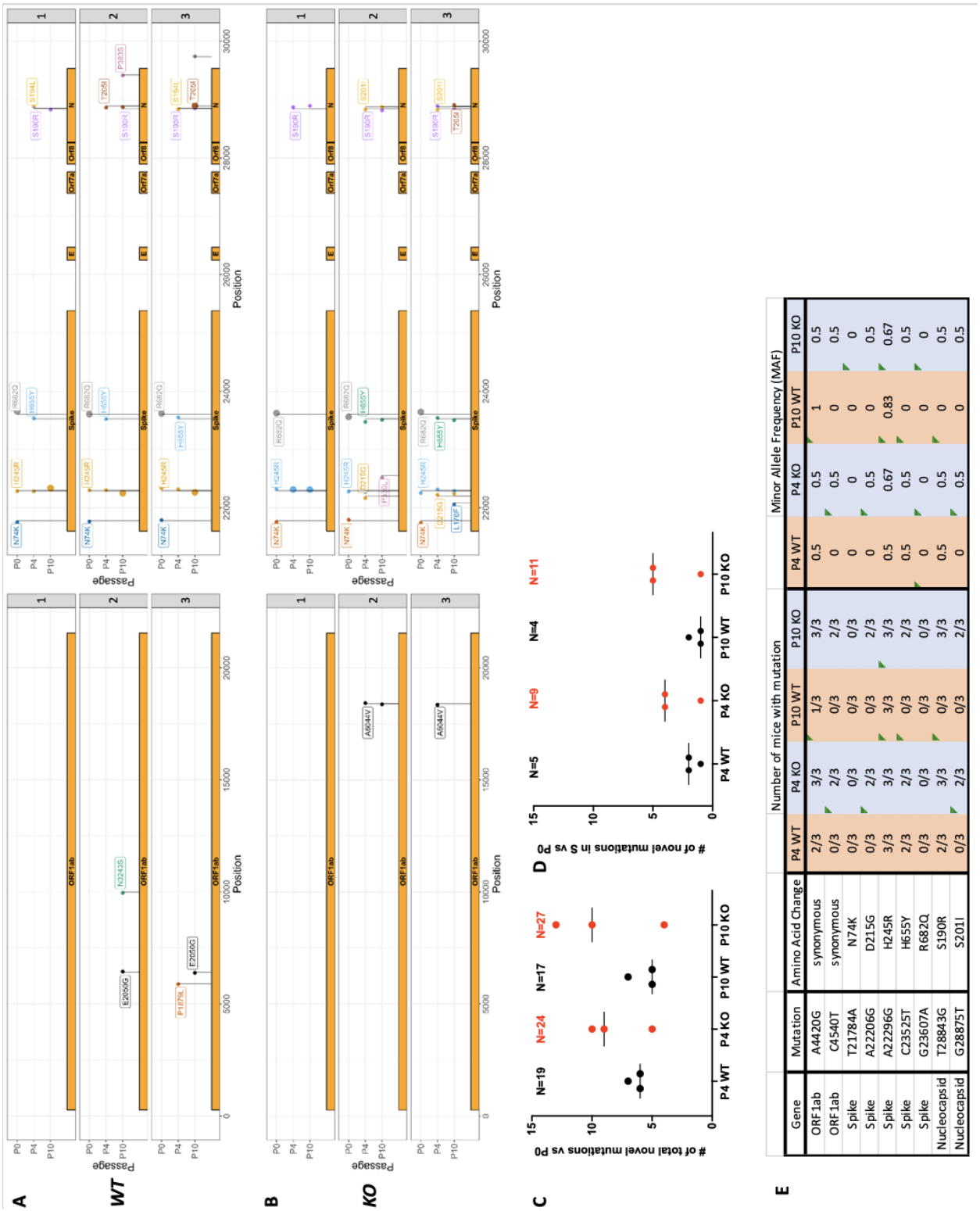

Gene	Mutation	Amino Acid Change	Number of mice with mutation				Minor Allele Frequency (MAF)			
			P4 WT	P4 KO	P10 WT	P10 KO	P4 WT	P4 KO	P10 WT	P10 KO
ORF1ab	A4420G	synonymous	2/3	3/3	1/3	3/3	0.5	0.5	1	0.5
ORF1ab	C4540T	synonymous	0/3	2/3	0/3	2/3	0	0.5	0	0.5
Spike	T21784A	N74K	0/3	0/3	0/3	0/3	0	0	0	0
Spike	A22206G	D215G	0/3	2/3	0/3	2/3	0	0.5	0	0.5
Spike	A22296G	H245R	3/3	3/3	3/3	3/3	0.5	0.67	0.83	0.67
Spike	C23525T	H655Y	2/3	2/3	0/3	2/3	0.5	0.5	0	0.5
Spike	G23607A	R682Q	0/3	0/3	0/3	0/3	0	0	0	0
Nucleocapsid	T28843G	S190R	2/3	3/3	0/3	3/3	0.5	0.5	0	0.5
Nucleocapsid	G28875T	S201I	0/3	2/3	0/3	2/3	0	0.5	0	0.5

Figure 5: Different mutational profile between SARS-CoV-2 passaged in male SAP KO and WT mice at P4 and P10. **(A)** Mutational profile of viruses passaged in SAP WT along the SARS-CoV-

2 genome (n=3 lineages). **(B)** Mutational profile of viruses passaged in SAP KO along the SARS-CoV-2 genome (n=3 lineages). For both **A)** and **B),** missense variants are shown. **(C)** Number of novel mutations across the SARS-CoV-2 genome compared to the P0 stock (n=3 per mouse genotype, per passage number) . **(D)** Number of novel mutations across in the spike gene compared to the P0 stock (n=3 per mouse genotype, per passage number). For **(C)** and **(D),** the total aggregated number of mutations for SAP KO and WT passaged virus lineages at P4 and P10 are displayed. **(E)** Mutations of interest: the gene, mutation, amino acid change, number of lineages per mouse genotype with mutation (shown as "number of mice with mutation"), where orange is SAP WT passaged viruses and blue is SAP KO passaged viruses, minor allele frequencies of mutations are shown.

Chapter IV: Discussion

In this study, the first objective was to compare the dynamics of SARS-CoV-2 infection in SAP deficient, K18-hACE2 hemizygous mice (SAP KO) with K18-hACE2 hemizygous mice (SAP WT). It was hypothesized that SAP WT mice would have a less severe phenotype in response to SARS-CoV-2 infection, compared to SAP KO mice, ultimately resulting from a differential cell immune response.

To address this hypothesis, we first sought to evaluate the clinical phenotype in SAP KO and WT mice following intranasal infection with a low (50 PFU/mouse), medium (5000 PFU/mouse) and a high dose (25000 PFU/mouse) of SARS-CoV-2, that was originally clinically isolated in Montreal before November 2021. After monitoring survival of mice following infection, both SAP KO and WT developed severe disease at all three doses, with no clinical differences noted between both groups. Both of these cohorts infected with a low dose started succumbing at 6 DPI with the last mouse succumbing at 9 DPI. In the literature, it has been reported that approximately 50% of K18-hACE2 mice infected with 2×10^1 or 2×10^2 PFU/mouse of SARS-CoV-2 WA1/2020 (one of the earliest strains of SARS-CoV-2, isolated in January 2020) succumbed by 10 DPI. Next, for infections at a medium dose, we observed that mice from both genotypes succumbed between 5 DPI and 6 DPI; and those infected with a high dose all succumbed at 5 DPI. In comparison, it has been reported that approximately 90% of K18-hACE2 mice infected with 2×10^3 and 2×10^4 PFU/mouse succumbed by 7 DPI. The difference between the literature and our findings might be explained by the different strains of SARS-CoV-2 used for infections, especially since our variant contained several mutations compared to the ancestral strain of SARS-CoV-2, namely the D614G amino acid substitution, which is known to promote viral fitness by increasing cellular entry efficiency with enhanced ACE2 entry [127,128].

Furthermore, upon investigating the histopathology of lungs from infected mice, interstitial pneumonitis was observed at both low and medium doses in both SAP KO and WT at 6 DPI for low dose and 5 DPI for medium dose, however no differences in scores for neutrophils in alveolar and interstitial spaces, hyaline membranes, proteinaceous debris filling the airspaces, alveolar septal thickening or congestion was found. All in all, these results indicate that at the clinical level, there were no differences between SAP KO and WT mice at the evaluated doses.

We then investigated the viral load after infecting SAP KO and WT mice and did not find differences between infectious viral titres and viral spike expression in the lungs. It is worth noting that viral titres found in the lungs for the low dose inoculum at 6 DPI (~10^5 PFU/g) was comparable with that of the medium (~10^5 PFU/g) and high dose (10^5-10^6 PFU/g) infected SAP KO and WT mice at 5 DPI. In addition, no differences were noted between SAP KO and WT in the frontal lobe tissue of the brain, where (~10^8 PFU/g) was noted in both genotypes, at 6 DPI when infected with low dose, and at 5 DPI when infected with medium dose. These results are similar to literature findings where K18-hACE2 mice infected with 2.5×10^4 PFU/mouse had a viral titre of ~10^6 PFU/g at 4 DPI in the lung and ~10^8 PFU/g in the brain[15]. We also found that the level of expression of SARS-CoV-2 spike gene normalized against *Gapdh* was also similar between SAP KO and WT (10^3-10^4-fold change) at all doses evaluated. These results indicated that there was no difference in the ability to control the virus load between SAP KO and WT at the evaluated doses and times of infection, indicating that if any, the impact of SAP-deficiency was inapparent in the outcome of SARS-CoV-2 infection in the K18-hACE2 model. As mentioned in the **Introduction**, a limitation in the K18-hACE2 mouse model is the non-physiological expression of the hACE2 transgene, as it is driven by the K18 promoter and can be expressed in epithelial tissues other than endogenously expressed ACE2; it is independent of regulatory mechanisms that control expression of hACE2;

and 8 full copies are inserted in the mouse chromosome 2, despite being expressed on chromosome X in humans[15]. The the non-physiological abundance expression of hACE2 in different tissues, such as the brain, could explain the severe disease observed in both SAP KO and WT, which could have a "masking effect" of SAP deficiency in SAP KO mice[15,99]. However, despite this effect, there could still be differences noted at the molecular level regarding immune cells and expression of genes upon infection. This idea allowed us to pursue the next step which was to start investigating the immunological response to SARS-CoV-2. As it has been previously shown, mice with SAP deficiency have defective activation of NK cells; and hyperactivation of $CD8^+$ CTLs with increased secretion of IFNγ in response to LCMV and MHV68 infection[78-81]. This led us to investigate cellular markers of both NK and CD8 cells upon SARS-CoV-2 infection, especially in the case of the K18-hACE2 mice, where it has been shown that these cells are present on 4 DPI upon infection with 2.5×10^4 PFU/mouse[15]. By looking at the relative expression of the Natural Cytotoxicity Receptor (NCR) *Nkp46* which is conserved in all mammalian species[129], we did not find any difference between the SAP KO mice compared to SAP WT at the high dose of infection. In contrast, upon investigating the expression of *CD8α*, a gene expressed by $CD8^+$ T cells[126], we observed a trend toward increased *CD8α* expression in the lungs of SAP KO compared to WT mice at low and medium dose and a significant increase at high dose. This could suggest that a more $CD8^+$ cells are recruited in the lungs of infected SAP KO mice compared to SAP WT mice, however, to make such a conclusion requires an investigation of the individual cells using flow cytometric approaches.

We then looked at expression of *Ifnγ* in the lungs of infected SAP KO and SAP WT mice at all infected doses, where a similar trend toward increased *Ifnγ* expression was seen in SAP KO compared to SAP WT was observed. The trend observed with IFNγ was also seen upon looking at

the plasma cytokines of mice infected with medium dose at 5 DPI, and in the BAL fluid of mice infected with high dose at 5 DPI.

Furthermore, by looking at cytotoxic granules that are known to be released by NK and $CD8^+$ cells: *Gzmb* and *Prf1*, we also observed similar findings. The expression of both *Gzmb* and *Prf1* relative to *Gapdh* was significantly higher in SAP KO mice than WT at the highest dose of infection. Previously, acute infection of SAP deficient mice with LCMV and MHV68 led to an increased number of virus-specific $CD8^+$ T cells and production of IFNγ by these cells in SAP deficient mice[10,86], which is in agreement with the trend toward toward increase expression of *CD8α* and *Ifnγ* in the context of SARS-CoV-2.

The next step to validate these results would be to look at the CD8+ and NK cells expressing *Ifnγ*, *Gzmb* and *Prf1* proteins by flow cytometry. With the data shown in this thesis, there is a suggestion of differential immunological response upon infection with SARS-CoV-2 in SAP KO mice compared to SAP WT, at the transcriptional level of cellular and cytotoxic marker expression.

During the COVID-19 pandemic, there were several reports of chronically infected immunodeficient patients in which the virus was reported to evolve and lead to the emergence of variants of both biological and epidemiological relevance[35,70,71]. With this in hand, our second objective in this study was to then evaluate the effect of SAP on the viral evolution of SARS-CoV-2. Our hypothesis was that we would observe a different mutational profile between viruses passaged in SAP KO compared to SAP WT mice. To test our hypothesis, we serially passaged lung homogenates obtained from infected SAP KO and WT mice for ten rounds generating 3 distinct lineages per genotype. These homogenates were taken at 4 DPI in order to obtain a sufficiently high titers for subsequent passages and to capture NK and $CD8^+$ T cell responses, previously reported in K18-hACE2 mice. At 4 DPI, there were no significant differences in clinical

signs, body weight loss, viral titres and the titre of the initial inoculi across different passages and lineages of both SAP KO and WT mice, until P10. However, at P5, there was a trend toward higher clinical scores and body weight loss for SAP KO compared to SAP WT mice. The viral stock initially used for passaging, the lung homogenates of different lineages from P4, used as the inoculi for P5, as well as the last passage lung homogenates were sent for RNA sequencing and analysis.

Viral RNA sequencing at P4 and P10 revealed many interesting results, that agreed with our original hypothesis. Compared to the initial stock used for passaging experiments (P0), when the total number of mutations in SAP KO mice was compared to that of SAP WT mice, a trend toward a larger number of mutations was observed at both P4 and P10 for the SAP KO compared to SAP WT mice. Looking at the particular viral genes that harboured the most mutations, a trend toward more mutations in the spike gene was found in SAP KO mice compared to SAP WT at both P4 and P10. A previous study has shown that two SARS-CoV-2 spike peptides (133-FQFCND-138 and 537- **KCVNFNF**-543), were able to bind to the NKG2D receptor on NK cells *in vitro*, which led to the secretion of IFNγ and increased cytotoxicity against cancer cell lines in presence of the spike peptides[130]. Similarly, many SARS-CoV-2 spike epitopes presented on HLA alleles have also been shown to induce a $CD8^+$ CTL response in HLA transgenic mice[131]. Therefore, one plausible explanation to the increased number of mutations in the spike gene of SAP KO-passaged viruses compared to SAP WT could be due to selection by an increased number of NK and $CD8^+$ cells, which remains to be investigated.

Looking at the mutational profile of P4 and P10 viruses passaged in SAP KO and WT mice, the spike D215G and the nucleocapsid S201I coding amino acid substitutions appeared in 2 of 3 SAP KO mice at P4 and P10 but were absent in SAP WT mice. Interestingly, the spike D215G substitution is a defining mutation in the B.1.351 (beta) variant and has been shown to modestly

increase spike fusion to target cells *in vitro*. Furthermore, it has been shown to emerge in the rectal swab samples of non-human primates infected with SARS-CoV-2 for a 4 week period[132]. However, no information is currently known about the role of the S201I nucleocapsid substitution. In addition, the 2 spike amino acid substitutions N74K and R682Q present in the P0 were no longer detected in all sequenced viruses at P4 and P10 passaged in both SAP KO and WT mice. One study showed that the R682Q variant, which occurs at the S1/S2 cleavage site, emerged during the *in vitro* passaging of the virus in VeroE6 cells[133]. Another study also reported the emergence of the NTD N74K spike substitution upon viral passaging *in vitro*, where it was increased the positive charge of the surface of the NTD[134]. Therefore, the disappearance of these mutations upon *in vivo* passaging, could be explained by their VeroE6 cell-specificity. Moreover, some mutations appeared in both SAP KO and WT viral lineages at P4 and disappeared in the SAP WT for P10 lineages. This is the case of the spike H655Y substitution which appeared in 2/3 of SAP KO and SAP WT viral lineages at P4 and was detected in 3/3 of SAP KO lineage and undetected in the SAP WT lineage at P10. The H655Y is found in the S2 domain, is a defining mutation in the P.1 (gamma) and omicron lineage VOCs and is known to reduce SARS-CoV-2 plasma membrane entry and facilitate endosomal entry[135]. It has also been reported to emerge in animal species disease models, including cats and non-human primates[132,136]. In fact, it has been shown to increase transmission in Syrian golden hamsters and display an enhanced infection phenotype in a human primary airway model[137]. Moreover, one study revealed that the H655Y substitution induced T-cell response in C57BL/6 mice vaccinated with an adenovirus type 5 vector encoding the Omicron BA.1 spike[138]. The latter could be an explanation for why there is a favorable selection in SAP KO mice between P4 and P10, and not in SAP WT mice.

A common mutation in the spike was also detected in P4 and P10 for all SAP KO and WT mice but not in P0, the H245R variant which has been previously found to emerge in cell culture passaging. A possible explanation for this could be that the variant emerged in cell culture but was detected at a frequency less than 20%, which is the cut-off used for detecting variants in this study. Subsequently, after passaging in both SAP KO and WT mice was increased which could be due to the mouse-specific adaptions.

Therefore, one limitation encountered in our sequencing analysis was that viral quasi-species occurring at frequency less than 20% were not detected. A more stringent analysis could be performed to reveal these low frequency variants. Finally, an additional layer of evidence by long-read sequencing will be next performed. These results suggest a differential immune response and viral selection pressures found in SAP deficient mice infected with SARS-CoV-2.

Limitations and Future Directions

Although of interest, this study on the role of SAP in the host response and intra-host evolution of SARS-CoV-2 has some limitations. Firstly, the number of mice used for our studies can be increased in order to make stronger conclusions, especially in the context of studying viral evolution. Second, the immune response studied here is based on gene expression of certain markers by qPCR; a future direction of this research would be to address the cellular response and expression cytotoxic effector molecules (IFNγ, GZMB and PRF1) secreted by $CD8^+$ T cells and NK cells by flow cytometry. Third, we did not observe clinical differences between SAP KO and WT with the K18-hACE2 background, most likely due to the overexpression of hACE2, as mentioned earlier.

A future direction of this research would be to infect SAP deficient mice (without the K18-hACE2 transgene) with mouse-adapted strains of SARS-CoV-2[96-100]. Alternatively, another approach could be to transiently express hACE2 in lung tissues SAP deficient mice (without the K18-hACE2 transgene) by adenovirus or adeno-associated viral transduction before infection with SARS-CoV-2[102-104]. Another important point to highlight is that our viral sequencing approach (Illumina) can yield short reads which may result in gaps and missasemblies[139]. Alternatively, Nanopore sequencing can detect long reads and de novo viral genome assembly, copy number alterations and complex structural variations [139]. Therefore, our results will be validated once again by Illumina and by Nanopore sequencing to confirm the mutational profile we observed in our studies. More viral passaging can be performed in order monitor the emergence of more viral variants in both SAP KO and SAP WT viral lineages, however it is important to be aware of concerns surrounding the topic of Gain-of-Function research, especially since in this case, a human virus (SARS-CoV-2) is passaged in humanized mice (expressing hACE2)[140].

Conclusions & Summary

In this study, we have studied the role of SAP in host response and investigated host evolution. Despite not seeing clinical and virological differences in SAP KO compared to SAP WT mice, we did see differences at the gene expression of immune genes (*CD8α*, *IFNγ*, *GZMB*, *Prf1*), as well as some mutational differences between SAP KO and WT passaged viruses, suggesting a differential immune response and viral selection pressures in SAP deficiency.

List of References

1 World Health Organization. *Weekly epidemiological update on COVID-19 - 15 June 2023*, <https://www.who.int/publications/m/item/weekly-epidemiological-update-on-covid-19---15-june-2023> (2023).

2 Mancini, M. & Vidal, S. M. Mechanisms of Natural Killer Cell Evasion Through Viral Adaptation. *Annual Review of Immunology* **38**, 511-539 (2020). https://doi.org:10.1146/annurev-immunol-082619-124440

3 Hoffmann, C. *et al.* Immune deficiency is a risk factor for severe COVID-19 in people living with HIV. *HIV Medicine* **22**, 372-378 (2021). https://doi.org:10.1111/hiv.13037

4 Jones, J. M., Faruqi, A. J., Sullivan, J. K., Calabrese, C. & Calabrese, L. H. COVID-19 Outcomes in Patients Undergoing B Cell Depletion Therapy and Those with Humoral Immunodeficiency States: A Scoping Review. *Pathog Immun* **6**, 76-103 (2021). https://doi.org:10.20411/pai.v6i1.435

5 Liu, B. M. & Hill, H. R. Role of Host Immune and Inflammatory Responses in COVID-19 Cases with Underlying Primary Immunodeficiency: A Review. *Journal of Interferon & Cytokine Research* **40**, 549-554 (2020). https://doi.org:10.1089/jir.2020.0210

6 Gao, Y., Chen, Y., Liu, M., Shi, S. & Tian, J. Impacts of immunosuppression and immunodeficiency on COVID-19: A systematic review and meta-analysis. *J Infect* **81**, e93-e95 (2020). https://doi.org:10.1016/j.jinf.2020.05.017

7 Tangye, S. G. XLP: Clinical Features and Molecular Etiology due to Mutations in SH2D1A Encoding SAP. *Journal of Clinical Immunology* **34**, 772-779 (2014). https://doi.org:10.1007/s10875-014-0083-7

8 Gartshteyn, Y., Askanase, A. D. & Mor, A. SLAM Associated Protein Signaling in T Cells: Tilting the Balance Toward Autoimmunity. *Frontiers in Immunology* **12** (2021). https://doi.org:10.3389/fimmu.2021.654839

9 Sintes, J., Romero, X., Marin, P., Terhorst, C. & Engel, P. Differential expression of CD150 (SLAM) family receptors by human hematopoietic stem and progenitor cells. *Experimental Hematology* **36**, 1199-1204 (2008). https://doi.org:https://doi.org/10.1016/j.exphem.2008.03.015

10 Wu, C. *et al.* SAP controls T cell responses to virus and terminal differentiation of TH2 cells. *Nature Immunology* **2**, 410-414 (2001). https://doi.org:10.1038/87713

11 Chen, G. *et al.* Increased proliferation of CD8+ T cells in SAP-deficient mice is associated with impaired activation-induced cell death. *European Journal of Immunology* **37**, 663-674 (2007). https://doi.org:https://doi.org/10.1002/eji.200636417

12 Pasquier, B. *et al.* Defective NKT cell development in mice and humans lacking the adapter SAP, the X-linked lymphoproliferative syndrome gene product. *Journal of Experimental Medicine* **201**, 695-701 (2005). https://doi.org:10.1084/jem.20042432

13 Di Vito, C. *et al.* Natural Killer Cells in SARS-CoV-2 Infection: Pathophysiology and Therapeutic Implications. *Frontiers in Immunology* **13** (2022). https://doi.org:10.3389/fimmu.2022.888248

14 Sette, A. & Crotty, S. Adaptive immunity to SARS-CoV-2 and COVID-19. *Cell* **184**, 861-880 (2021). https://doi.org:https://doi.org/10.1016/j.cell.2021.01.007

15 Winkler, E. S. *et al.* SARS-CoV-2 infection of human ACE2-transgenic mice causes severe lung inflammation and impaired function. *Nature Immunology* **21**, 1327-1335 (2020). https://doi.org:10.1038/s41590-020-0778-2
16 Wang, C., Horby, P. W., Hayden, F. G. & Gao, G. F. A novel coronavirus outbreak of global health concern. *The Lancet* **395**, 470-473 (2020). https://doi.org:10.1016/S0140-6736(20)30185-9
17 Wang, H. *et al.* The genetic sequence, origin, and diagnosis of SARS-CoV-2. *Eur J Clin Microbiol Infect Dis* **39**, 1629-1635 (2020). https://doi.org:10.1007/s10096-020-03899-4
18 Willett, B. J. *et al.* SARS-CoV-2 Omicron is an immune escape variant with an altered cell entry pathway. *Nature Microbiology* **7**, 1161-1179 (2022). https://doi.org:10.1038/s41564-022-01143-7
19 Alam, M. S. Insight into SARS-CoV-2 Omicron variant immune escape possibility and variant independent potential therapeutic opportunities. *Heliyon* **9(2)** e13285 (2023). https://doi.org:10.1016/j.heliyon.2023.e13285
20 (NIH), N. H. I. *Clinical Spectrum of SARS-CoV-2 Infection* , <https://www.covid19treatmentguidelines.nih.gov/overview/clinical-spectrum/> (2023).
21 Cobat, A. *et al.* Human Genomics of COVID-19 Pneumonia: Contributions of Rare and Common Variants. *Annual Review of Biomedical Data Science* (2023). https://doi.org:10.1146/annurev-biodatasci-020222-021705
22 Guimarães, D., Pissarra, R., Reis-Melo, A. & Guimarães, H. Multisystem inflammatory syndrome in children (MISC): A systematic review. *International Journal of Clinical Practice* **75**, e14450 (2021). https://doi.org:https://doi.org/10.1111/ijcp.14450
23 Davis, H. E., McCorkell, L., Vogel, J. M. & Topol, E. J. Long COVID: major findings, mechanisms and recommendations. *Nature Reviews Microbiology* **21**, 133-146 (2023). https://doi.org:10.1038/s41579-022-00846-2
24 Paludan, S. R. & Mogensen, T. H. Innate immunological pathways in COVID-19 pathogenesis. *Science Immunology* **7**, eabm5505 https://doi.org:10.1126/sciimmunol.abm5505
25 Liao, M. *et al.* Single-cell landscape of bronchoalveolar immune cells in patients with COVID-19. *Nat Med* **26**, 842-844 (2020). https://doi.org:10.1038/s41591-020-0901-9
26 Wauters, E. *et al.* Discriminating mild from critical COVID-19 by innate and adaptive immune single-cell profiling of bronchoalveolar lavages. *Cell Research* **31**, 272-290 (2021). https://doi.org:10.1038/s41422-020-00455-9
27 Reusch, N. *et al.* Neutrophils in COVID-19. *Frontiers in Immunology* **12** (2021). https://doi.org:10.3389/fimmu.2021.652470
28 McKenna, E. *et al.* Neutrophils in COVID-19: Not Innocent Bystanders. *Frontiers in Immunology* **13** (2022). https://doi.org:10.3389/fimmu.2022.864387
29 van Erp, E. A., van Kampen, M. R., van Kasteren, P. B. & de Wit, J. Viral Infection of Human Natural Killer Cells. *Viruses* **11** (2019). https://doi.org:10.3390/v11030243
30 Duev-Cohen, A. *et al.* Altered NKp46 Recognition and Elimination of Influenza B Viruses. *Viruses* **13** (2020). https://doi.org:10.3390/v13010034
31 Kim, H. *et al.* SARS-CoV-2 peptides bind to NKG2D and increase NK cell activity. *Cell Immunol* **371**, 104454 (2022). https://doi.org:10.1016/j.cellimm.2021.104454
32 Malengier-Devlies, B. *et al.* Severe COVID-19 patients display hyper-activated NK cells and NK cell-platelet aggregates. *Front Immunol* **13**, 861251 (2022). https://doi.org:10.3389/fimmu.2022.861251

33 Hammer, Q. *et al.* SARS-CoV-2 Nsp13 encodes for an HLA-E-stabilizing peptide that abrogates inhibition of NKG2A-expressing NK cells. *Cell Reports* **38**, 110503 (2022). https://doi.org:10.1016/j.celrep.2022.110503
34 Agerer, B. *et al.* SARS-CoV-2 mutations in MHC-I-restricted epitopes evade CD8+ T cell responses. *Science Immunology* **6**, eabg6461 (2021). https://doi.org:10.1126/sciimmunol.abg6461
35 Markarian, N. M. *et al.* Identifying Markers of Emerging SARS-CoV-2 Variants in Patients With Secondary Immunodeficiency. *Frontiers in Microbiology* **13** (2022). https://doi.org:10.3389/fmicb.2022.933983
36 Boson, B. *et al.* The SARS-CoV-2 envelope and membrane proteins modulate maturation and retention of the spike protein, allowing assembly of virus-like particles. *Journal of Biological Chemistry* **296** (2021).
37 Banerjee, A., Doxey, A. C., Mossman, K. & Irving, A. T. Unraveling the Zoonotic Origin and Transmission of SARS-CoV-2. *Trends in Ecology & Evolution* **36**, 180-184 (2021). https://doi.org:10.1016/j.tree.2020.12.002
38 Wu, A. *et al.* Genome composition and divergence of the novel coronavirus (2019-nCoV) originating in China. *Cell Host & Microbe* **27**, 325-328 (2020).
39 V'kovski, P., Kratzel, A., Steiner, S., Stalder, H. & Thiel, V. Coronavirus biology and replication: implications for SARS-CoV-2. *Nature Reviews Microbiology* **19**, 155-170 (2021).
40 Wang, Q. *et al.* Structural basis for RNA replication by the SARS-CoV-2 polymerase. *Cell* **182**, 417-428. e413 (2020).
41 Wang, Y. *et al.* Human SARS-CoV-2 has evolved to reduce CG dinucleotide in its open reading frames. *Scientific Reports* **10(1):12331**, 1-10 (2020).
42 Yan, L. *et al.* Cryo-EM structure of an extended SARS-CoV-2 replication and transcription complex reveals an intermediate state in cap synthesis. *Cell* **184**, 184-193. e110 (2021).
43 Davidson, A. D. *et al.* Characterisation of the transcriptome and proteome of SARS-CoV-2 reveals a cell passage induced in-frame deletion of the furin-like cleavage site from the spike glycoprotein. *Genome Medicine* **12**, 1-15 (2020).
44 Jiang, H. W. *et al.* SARS-CoV-2 Orf9b suppresses type I interferon responses by targeting TOM70. *Cellular & Molecular Immunology* **17**, 998-1000 (2020). https://doi.org:10.1038/s41423-020-0514-8
45 Michel, C. J., Mayer, C., Poch, O. & Thompson, J. D. Characterization of accessory genes in coronavirus genomes. *Virology Journal* **17**, 131 (2020). https://doi.org:10.1186/s12985-020-01402-1
46 Mohammad, S. *et al.* SARS-CoV-2 ORF8 and SARS-CoV ORF8ab: Genomic Divergence and Functional Convergence. *Pathogens* **9** (2020). https://doi.org:10.3390/pathogens9090677
47 Pancer, K. *et al.* The SARS-CoV-2 ORF10 is not essential in vitro or in vivo in humans. *PLoS Pathogens* **16**, e1008959 (2020). https://doi.org:10.1371/journal.ppat.1008959
48 Conceicao, C. *et al.* The SARS-CoV-2 Spike protein has a broad tropism for mammalian ACE2 proteins. *PLoS Biol* **18**, e3001016 (2020). https://doi.org:10.1371/journal.pbio.3001016
49 Huang, Y., Yang, C., Xu, X. F., Xu, W. & Liu, S. W. Structural and functional properties of SARS-CoV-2 spike protein: potential antivirus drug development for COVID-19. *Acta*

Pharmacologica Sinica **41**, 1141-1149 (2020). https://doi.org:10.1038/s41401-020-0485-4

50 Marti, D., Torras, J., Bertran, O., Turon, P. & Aleman, C. Temperature effect on the SARS-CoV-2: A molecular dynamics study of the spike homotrimeric glycoprotein. *Computational and Structural Biotechnology Journal* **19**, 1848-1862 (2021).

51 Kakavandi, S. *et al.* Structural and non-structural proteins in SARS-CoV-2: potential aspects to COVID-19 treatment or prevention of progression of related diseases. *Cell Communication and Signaling* **21**, 110 (2023). https://doi.org:10.1186/s12964-023-01104-5

52 Li, M. Y., Li, L., Zhang, Y. & Wang, X. S. Expression of the SARS-CoV-2 cell receptor gene ACE2 in a wide variety of human tissues. *Infectious Diseases of Poverty* **9**, 45 (2020). https://doi.org:10.1186/s40249-020-00662-x

53 Ni, W. *et al.* Role of angiotensin-converting enzyme 2 (ACE2) in COVID-19. *Critical Care* **24**, 422 (2020). https://doi.org:10.1186/s13054-020-03120-0

54 Lopes-Pacheco, M. *et al.* Pathogenesis of multiple organ injury in COVID-19 and potential therapeutic strategies. *Frontiers in Physiology* **12**, 593223 (2021).

55 Astuti, I. & Ysrafil. Severe Acute Respiratory Syndrome Coronavirus 2 (SARS-CoV-2): An overview of viral structure and host response. *Diabetes & Metabolic Syndrome: Clinical Research & Reviews* **14**, 407-412 (2020). https://doi.org:10.1016/j.dsx.2020.04.020

56 Dampalla, C. S. *et al.* Postinfection treatment with a protease inhibitor increases survival of mice with a fatal SARS-CoV-2 infection. *Proceedings of the National Academy of Sciences* **118** (2021). https://doi.org:10.1073/pnas.2101555118

57 Roe, M. K., Junod, N. A., Young, A. R., Beachboard, D. C. & Stobart, C. C. Targeting novel structural and functional features of coronavirus protease nsp5 (3CLpro, Mpro) in the age of COVID-19. *The Journal of General Virology* **102** (2021).

58 Brant, A. C., Tian, W., Majerciak, V., Yang, W. & Zheng, Z. M. SARS-CoV-2: from its discovery to genome structure, transcription, and replication. *Cell & Bioscience* **11**, 136 (2021). https://doi.org:10.1186/s13578-021-00643-z

59 Malone, B., Urakova, N., Snijder, E. J. & Campbell, E. A. Structures and functions of coronavirus replication–transcription complexes and their relevance for SARS-CoV-2 drug design. *Nature Reviews Molecular Cell Biology* **23**, 21-39 (2022). https://doi.org:10.1038/s41580-021-00432-z

60 Shannon, A. *et al.* Remdesivir and SARS-CoV-2: Structural requirements at both nsp12 RdRp and nsp14 Exonuclease active-sites. *Antiviral Research* **178**, 104793 (2020). https://doi.org:10.1016/j.antiviral.2020.104793

61 Gribble, J. *et al.* The coronavirus proofreading exoribonuclease mediates extensive viral recombination. *PLoS Pathogens* **17**, e1009226 (2021). https://doi.org:10.1371/journal.ppat.1009226

62 Chen, J., Wang, R., Wang, M. & Wei, G. W. Mutations Strengthened SARS-CoV-2 Infectivity. *J Mol Biol* **432**, 5212-5226 (2020). https://doi.org:10.1016/j.jmb.2020.07.009

63 Ko, K. *et al.* Molecular characterization and the mutation pattern of SARS-CoV-2 during first and second wave outbreaks in Hiroshima, Japan. *PLoS One* **16**, e0246383 (2021). https://doi.org:10.1371/journal.pone.0246383

64 Dapp, M. J. *et al.* Patterns and rates of viral evolution in HIV-1 subtype B infected females and males. *PLoS One* **12**, e0182443 (2017). https://doi.org:10.1371/journal.pone.0182443
65 Simon-Loriere, E. & Holmes, E. C. Why do RNA viruses recombine? *Nature Reviews Microbiology* **9**, 617-626 (2011). https://doi.org:10.1038/nrmicro2614
66 Pollett, S. *et al.* A comparative recombination analysis of human coronaviruses and implications for the SARS-CoV-2 pandemic. *Scientific Reports* **11**, 17365 (2021). https://doi.org:10.1038/s41598-021-96626-8
67 Francisco, R. D. S., Jr. *et al.* Pervasive transmission of E484K and emergence of VUI-NP13L with evidence of SARS-CoV-2 co-infection events by two different lineages in Rio Grande do Sul, Brazil. *Virus Research* **296**, 198345 (2021). https://doi.org:10.1016/j.virusres.2021.198345
68 Gu, H. *et al.* Adaptation of SARS-CoV-2 in BALB/c mice for testing vaccine efficacy. *Science* **369**, 1603-1607 (2020). https://doi.org:10.1126/science.abc4730
69 Gandhi, S. *et al.* De novo emergence of a remdesivir resistance mutation during treatment of persistent SARS-CoV-2 infection in an immunocompromised patient: a case report. *Nature Communications* **13**, 1547 (2022). https://doi.org:10.1038/s41467-022-29104-y
70 Wilkinson, S. A. J. *et al.* Recurrent SARS-CoV-2 mutations in immunodeficient patients. *Virus Evolution* **8**, veac050 (2022). https://doi.org:10.1093/ve/veac050
71 Harari, S. *et al.* Drivers of adaptive evolution during chronic SARS-CoV-2 infections. *Nature Medicine* **28**, 1501-1508 (2022). https://doi.org:10.1038/s41591-022-01882-4
72 Purtilo, D. *et al.* X-LINKED RECESSIVE PROGRESSIVE COMBINED VARIABLE IMMUNODEFICIENCY (DUNCAN'S DISEASE). *The Lancet* **305**, 935-941 (1975). https://doi.org:https://doi.org/10.1016/S0140-6736(75)92004-8
73 Nichols, K. E. & Marsh, R. A. in *Stiehm's Immune Deficiencies* (eds Kathleen E. Sullivan & E. Richard Stiehm) 475-495 (Academic Press, 2014).
74 Veillette, A. Immune regulation by SLAM family receptors and SAP-related adaptors. *Nature Reviews Immunology* **6**, 56-66 (2006). https://doi.org:10.1038/nri1761
75 Hwang, P. M. *et al.* A "three-pronged" binding mechanism for the SAP/SH2D1A SH2 domain: structural basis and relevance to the XLP syndrome. *The Embo Journal* **21**, 314-323 (2002). https://doi.org:10.1093/emboj/21.3.314
76 Panchal, N., Booth, C., Cannons, J. L. & Schwartzberg, P. L. X-Linked Lymphoproliferative Disease Type 1: A Clinical and Molecular Perspective. *Frontiers in Immunology* **9**, 666 (2018). https://doi.org:10.3389/fimmu.2018.00666
77 Soy, M., Atagündüz, P., Atagündüz, I. & Sucak, G. T. Hemophagocytic lymphohistiocytosis: a review inspired by the COVID-19 pandemic. *Rheumatology International* **41**, 7-18 (2021). https://doi.org:10.1007/s00296-020-04636-y
78 Cannons, J. L. *et al.* SAP regulates T cell-mediated help for humoral immunity by a mechanism distinct from cytokine regulation. *Journal of Experimental Medicine* **203**, 1551-1565 (2006). https://doi.org:10.1084/jem.20052097
79 McCausland, M. M. *et al.* SAP regulation of follicular helper CD4 T cell development and humoral immunity is independent of SLAM and Fyn kinase. *Journal of Immunology* **178**, 817-828 (2007). https://doi.org:10.4049/jimmunol.178.2.817
80 Kamperschroer, C., Dibble, J. P., Meents, D. L., Schwartzberg, P. L. & Swain, S. L. SAP Is Required for Th Cell Function and for Immunity to Influenza1. *The Journal of Immunology* **177**, 5317-5327 (2006). https://doi.org:10.4049/jimmunol.177.8.5317

81 Kim, I.-J. *et al.* Perturbation of B Cell Activation in SLAM-Associated Protein-Deficient Mice Is Associated with Changes in Gammaherpesvirus Latency Reservoirs1. *The Journal of Immunology* **178**, 1692-1701 (2007). https://doi.org:10.4049/jimmunol.178.3.1692

82 Ma, C. S. *et al.* Impaired humoral immunity in X-linked lymphoproliferative disease is associated with defective IL-10 production by CD4+ T cells. *Journal of Clinical Investigation* **115**, 1049-1059 (2005). https://doi.org:10.1172/jci23139

83 Dong, Z. *et al.* The Adaptor SAP Controls NK Cell Activation by Regulating the Enzymes Vav-1 and SHIP-1 and by Enhancing Conjugates with Target Cells. *Immunity* **36**, 974-985 (2012). https://doi.org:10.1016/j.immuni.2012.03.023

84 Bloch-Queyrat, C. *et al.* Regulation of natural cytotoxicity by the adaptor SAP and the Src-related kinase Fyn. *Journal of Experimental Medicine* **202**, 181-192 (2005). https://doi.org:10.1084/jem.20050449

85 Nakajima, H. *et al.* Patients with X-linked lymphoproliferative disease have a defect in 2B4 receptor-mediated NK cell cytotoxicity. *European Journal of Immunology* **30**, 3309-3318 (2000). https://doi.org:https://doi.org/10.1002/1521-4141(200011)30:11<3309::AID-IMMU3309>3.0.CO;2-3

86 Czar, M. J. *et al.* Altered lymphocyte responses and cytokine production in mice deficient in the X-linked lymphoproliferative disease gene SH2D1A/DSHP/SAP. *Proceedings of the National Academy of Sciences* **98**, 7449-7454 (2001). https://doi.org:10.1073/pnas.131193098

87 Crotty, S., McCausland, M. M., Aubert, R. D., Wherry, E. J. & Ahmed, R. Hypogammaglobulinemia and exacerbated CD8 T-cell–mediated immunopathology in SAP-deficient mice with chronic LCMV infection mimics human XLP disease. *Blood* **108**, 3085-3093 (2006). https://doi.org:10.1182/blood-2006-04-018929

88 Sharifi, R. *et al.* SAP mediates specific cytotoxic T-cell functions in X-linked lymphoproliferative disease. *Blood* **103**, 3821-3827 (2004). https://doi.org:10.1182/blood-2003-09-3359

89 Dupré, L. c. *et al.* SAP controls the cytolytic activity of CD8+ T cells against EBV-infected cells. *Blood* **105**, 4383-4389 (2005). https://doi.org:10.1182/blood-2004-08-3269

90 Chung, B., Aoukaty, A., Dutz, J., Terhorst, C. & Tan, R. Cutting Edge: Signaling Lymphocytic Activation Molecule-Associated Protein Controls NKT Cell Functions 1. *The Journal of Immunology* **174**, 3153-3157 (2005). https://doi.org:10.4049/jimmunol.174.6.3153

91 Nichols, K. E. *et al.* Regulation of NKT cell development by SAP, the protein defective in XLP. *Nature Medicine* **11**, 340-345 (2005). https://doi.org:10.1038/nm1189

92 Meazza, R. *et al.* Diagnosing XLP1 in patients with hemophagocytic lymphohistiocytosis. *Journal of Allergy and Clinicinal Immunology* **134**, 1381-1387.e1387 (2014). https://doi.org:10.1016/j.jaci.2014.04.043

93 Chung, M. H. *et al.* Fatal SARS in X-Linked Lymphoproliferative Disease Type 1: A Case Report. *Frontiers in Pediatrics* **10** (2022). https://doi.org:10.3389/fped.2022.794110

94 Prader, S. *et al.* X-Linked Lymphoproliferative Disease Mimicking Multisystem Inflammatory Syndrome in Children—A Case Report. *Frontiers in Pediatrics* **9** (2021). https://doi.org:10.3389/fped.2021.691024

95 Fan, C. *et al.* Animal models for COVID-19: advances, gaps and perspectives. *Signal Transduction and Targeted Therapy* **7**, 220 (2022). https://doi.org:10.1038/s41392-022-01087-8
96 Leist, S. R. *et al.* A Mouse-Adapted SARS-CoV-2 Induces Acute Lung Injury and Mortality in Standard Laboratory Mice. *Cell* **183**, 1070-1085 (2020). https://doi.org:https://doi.org/10.1016/j.cell.2020.09.050
97 Iwata-Yoshikawa, N. *et al.* A lethal mouse model for evaluating vaccine-associated enhanced respiratory disease during SARS-CoV-2 infection. *Science Advances* **8**, eabh3827 (2022) https://doi.org:10.1126/sciadv.abh3827
98 Dinnon, K. H. *et al.* SARS-CoV-2 infection produces chronic pulmonary epithelial and immune cell dysfunction with fibrosis in mice. *Science Translational Medicine* **14**, eabo5070 (2022) https://doi.org:10.1126/scitranslmed.abo5070
99 Beer, J. *et al.* Impaired immune response drives age-dependent severity of COVID-19. *Journal of Experimental Medicine* **219**, e20220621 (2022). https://doi.org:10.1084/jem.20220621
100 Zhang, Y. *et al.* SARS-CoV-2 rapidly adapts in aged BALB/c mice and induces typical pneumonia. *J Virol* **95** (2021). https://doi.org:10.1128/jvi.02477-20
101 Chu, H., Chan, J. F.-W. & Yuen, K.-Y. Animal models in SARS-CoV-2 research. *Nature Methods* **19**, 392-394 (2022). https://doi.org:10.1038/s41592-022-01447-w
102 Sun, J. *et al.* Generation of a Broadly Useful Model for COVID-19 Pathogenesis, Vaccination, and Treatment. *Cell* **182**, 734-743.e735 (2020). https://doi.org:https://doi.org/10.1016/j.cell.2020.06.010
103 Hassan, A. O. *et al.* A SARS-CoV-2 Infection Model in Mice Demonstrates Protection by Neutralizing Antibodies. *Cell* **182**, 744-753.e744 (2020). https://doi.org:https://doi.org/10.1016/j.cell.2020.06.011
104 Gary, E. N. *et al.* A novel mouse AAV6 hACE2 transduction model of wild-type SARS-CoV-2 infection studied using synDNA immunogens. *iScience* **24**, 102699 (2021). https://doi.org:https://doi.org/10.1016/j.isci.2021.102699
105 Winkler Emma, S. *et al.* SARS-CoV-2 Causes Lung Infection without Severe Disease in Human ACE2 Knock-In Mice. *Journal of Virology* **96**, e01511-01521 (2022). https://doi.org:10.1128/JVI.01511-21
106 Sun, S.-H. *et al.* A Mouse Model of SARS-CoV-2 Infection and Pathogenesis. *Cell Host & Microbe* **28**, 124-133.e124 (2020). https://doi.org:https://doi.org/10.1016/j.chom.2020.05.020
107 Dong, W. *et al.* The K18-Human ACE2 Transgenic Mouse Model Recapitulates Non-severe and Severe COVID-19 in Response to an Infectious Dose of the SARS-CoV-2 Virus. *Journal of Virology* **96**, e00964-00921 (2022). https://doi.org:10.1128/JVI.00964-21
108 Oladunni, F. S. *et al.* Lethality of SARS-CoV-2 infection in K18 human angiotensin-converting enzyme 2 transgenic mice. *Nature Communications* **11**, 6122 (2020). https://doi.org:10.1038/s41467-020-19891-7
109 Villadiego, J. *et al.* Full protection from SARS-CoV-2 brain infection and damage in susceptible transgenic mice conferred by MVA-CoV2-S vaccine candidate. *Nature Neuroscience* **26**, 226-238 (2023). https://doi.org:10.1038/s41593-022-01242-y
110 Shuai, H. *et al.* Emerging SARS-CoV-2 variants expand species tropism to murines. *eBioMedicine* **73** (2021). https://doi.org:10.1016/j.ebiom.2021.103643

111 Yang, J.-H. *et al.* Delta (B1.617.2) variant of SARS-CoV-2 induces severe neurotropic patterns in K18-hACE2 mice. *Scientific Reports* **13**, 3303 (2023). https://doi.org:10.1038/s41598-023-29909-x
112 Ying, B. *et al.* Boosting with variant-matched or historical mRNA vaccines protects against Omicron infection in mice. *Cell* **185**, 1572-1587.e1511 (2022). https://doi.org:10.1016/j.cell.2022.03.037
113 An, D. *et al.* Protection of K18-hACE2 mice and ferrets against SARS-CoV-2 challenge by a single-dose mucosal immunization with a parainfluenza virus 5-based COVID-19 vaccine. *Science Advances* **7(**27):eabi5246 (2021). https://doi.org:10.1126/sciadv.abi5246
114 Zhao, Y. *et al.* Vaccination with Span, an antigen guided by SARS-CoV-2 S protein evolution, protects against challenge with viral variants in mice. *Science Translational Medicine* **15**, eabo3332 https://doi.org:10.1126/scitranslmed.abo3332
115 Cáceres, C. J. *et al.* Efficacy of GC-376 against SARS-CoV-2 virus infection in the K18 hACE2 transgenic mouse model. *Scientific Reports* **11**, 9609 (2021). https://doi.org:10.1038/s41598-021-89013-w
116 Jeong, J. H. *et al.* Combination therapy with nirmatrelvir and molnupiravir improves the survival of SARS-CoV-2 infected mice. *Antiviral Research* **208**, 105430 (2022). https://doi.org:10.1016/j.antiviral.2022.105430
117 Fumagalli, V. *et al.* Nirmatrelvir treatment of SARS-CoV-2-infected mice blunts antiviral adaptive immune responses. *EMBO Molecular Medicine* **15**, e17580 (2023). https://doi.org:https://doi.org/10.15252/emmm.202317580
118 Yin, L. *et al.* Mice deficient in the X-linked lymphoproliferative disease gene sap exhibit increased susceptibility to murine gammaherpesvirus-68 and hypo-gammaglobulinemia. *J Med Virol* **71**, 446-455 (2003). https://doi.org:10.1002/jmv.10504
119 Javadi, A. *et al.* Qualification study of two genomic DNA extraction methods in different clinical samples. *Tanaffos* **13**, 41-47 (2014).
120 The Jackson Laboratory. *B6.Cg-Tg(K18-ACE2)2Prlmn/J*, <https://www.jax.org/Protocol?stockNumber=034860&protocolID=38275> (2023).
121 Patel, Dhanesh. New human angiotensin converting enzyme 2 (ACE2) knock-in CD-1 mouse model of asymptomatic SARS-CoV-2 infection. *McGill University* (Canada), 2022.
122 Amarilla, A. A. *et al.* An Optimized High-Throughput Immuno-Plaque Assay for SARS-CoV-2. *Frontiers in Microbiology* **12** (2021). https://doi.org:10.3389/fmicb.2021.625136
123 Reed, L. J. & Muench, H. A SIMPLE METHOD OF ESTIMATING FIFTY PER CENT ENDPOINTS. *American Journal of Epidemiology* **27**, 493-497 (1938). https://doi.org:10.1093/oxfordjournals.aje.a118408
124 Willett, J. D. S. *et al.* SARS-CoV-2 variant natural evolution in K18-ACE2 mice increases virulence and produces treatment resistance-linked variant alleles. *bioRxiv*, 2023.2001.2016.523994 (2023). https://doi.org:10.1101/2023.01.16.523994
125 Bezman, N. A. *et al.* Molecular definition of the identity and activation of natural killer cells. *Nature Immunology* **13**, 1000-1009 (2012). https://doi.org:10.1038/ni.2395
126 Hassan, H. *et al.* Cd8 enhancer E8I and Runx factors regulate CD8α expression in activated CD8+ T cells. *Proceedings of the National Academy of Sciences* **108**, 18330-18335 (2011). https://doi.org:10.1073/pnas.1105835108

127 Zhang, L. *et al.* SARS-CoV-2 spike-protein D614G mutation increases virion spike density and infectivity. *Nature Communications* **11**, 6013 (2020). https://doi.org:10.1038/s41467-020-19808-4
128 Ozono, S. *et al.* SARS-CoV-2 D614G spike mutation increases entry efficiency with enhanced ACE2-binding affinity. *Nature Communications* **12**, 848 (2021). https://doi.org:10.1038/s41467-021-21118-2
129 Barrow, A. D., Martin, C. J. & Colonna, M. The Natural Cytotoxicity Receptors in Health and Disease. *Frontiers in Immunology* **10** (2019). https://doi.org:10.3389/fimmu.2019.00909
130 Kim, H. *et al.* SARS-CoV-2 peptides bind to NKG2D and increase NK cell activity. *Cellular Immunology* **371**, 104454 (2022). https://doi.org:https://doi.org/10.1016/j.cellimm.2021.104454
131 Jin, X. *et al.* Screening HLA-A-restricted T cell epitopes of SARS-CoV-2 and the induction of CD8+ T cell responses in HLA-A transgenic mice. *Cellular & Molecular Immunology* **18**, 2588-2608 (2021). https://doi.org:10.1038/s41423-021-00784-8
132 Rowe, L. A. *et al.* Intra-Host SARS-CoV-2 Evolution in the Gut of Mucosally-Infected Chlorocebus aethiops (African Green Monkeys). *Viruses* **14** (2022).
133 Ogando, N. S. *et al.* SARS-coronavirus-2 replication in Vero E6 cells: replication kinetics, rapid adaptation and cytopathology. *Journal of General Virology* **101**, 925-940 (2020). https://doi.org:https://doi.org/10.1099/jgv.0.001453
134 Shiliaev, N. *et al.* Natural and recombinant SARS-CoV-2 isolates rapidly evolve in vitro to higher infectivity through more efficient binding to heparan sulfate and reduced S1/S2 cleavage. *Journal of Virology* **95**, e01357-01321 (2021).
135 Hu, B. *et al.* Spike mutations contributing to the altered entry preference of SARS-CoV-2 omicron BA.1 and BA.2. *Emerging Microbes & Infections* **11**, 2275-2287 (2022). https://doi.org:10.1080/22221751.2022.2117098
136 Braun, K. M. *et al.* Transmission of SARS-CoV-2 in domestic cats imposes a narrow bottleneck. *PLoS Pathogens* **17**, e1009373 (2021). https://doi.org:10.1371/journal.ppat.1009373
137 Escalera, A. *et al.* Mutations in SARS-CoV-2 variants of concern link to increased spike cleavage and virus transmission. *Cell Host & Microbe* **30**, 373-387.e377 (2022). https://doi.org:https://doi.org/10.1016/j.chom.2022.01.006
138 Wang, Y. *et al.* Effects of SARS-CoV-2 Omicron BA.1 Spike Mutations on T-Cell Epitopes in Mice. *Viruses* **15(3):763** (2023).
139 Tshiabuila, D. *et al.* Comparison of SARS-CoV-2 sequencing using the ONT GridION and the Illumina MiSeq. *BMC Genomics* **23**, 319 (2022). https://doi.org:10.1186/s12864-022-08541-5
140 Nicholas, G. E. & Charles, H. P. Gain-of-function research and model organisms in biology. *Journal of Medical Ethics*, jme-2022-108853 (2023). https://doi.org:10.1136/jme-2022-108853

Supplementary Figures

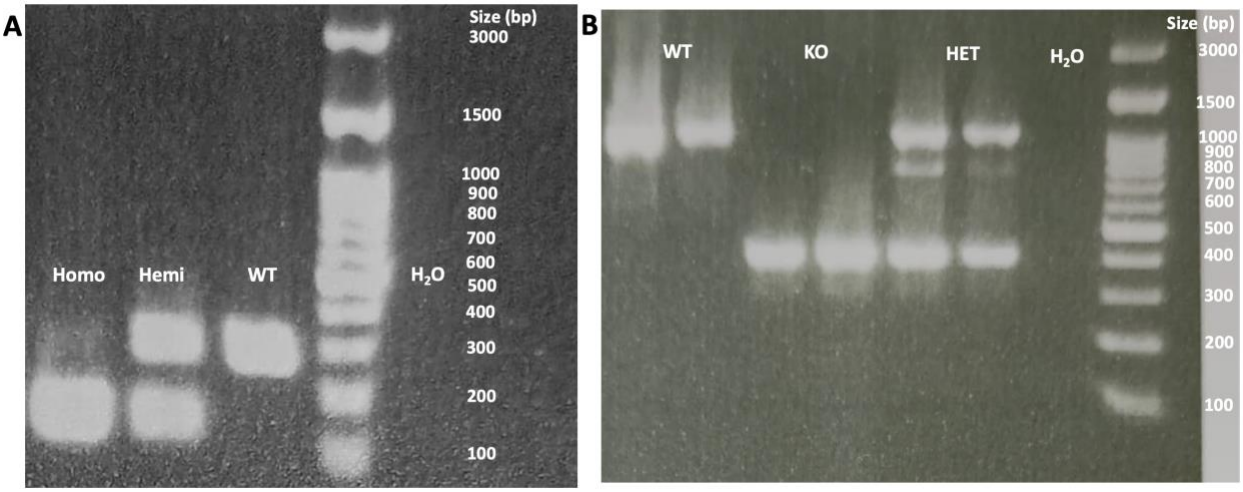

Supplementary Figure 1: Genotyping for K18-hACE2 and SAP in mice. **(A)** K18-hACE2 genotyping reveals 2 bands at 148 bp and 137 bp (seen as 1 band) for the homozygous genotype (shown as "Homo"), 3 bands at 285bp, 148 bp and 137 bp (seen as one band) for the hemizygous genotype (shown as "Hemi"), 1 band at 285bp for the wild type genotype (shown as WT). **(B)** SAP genotyping reveals 3 bands at 1083bp, 800bp and 400bp for the heterozygous genotype (shown as "Het"), one band at 1083bp for the wild type genotype (shown as "WT") and one band at 400bp for the mutant genotype (shown as "KO").

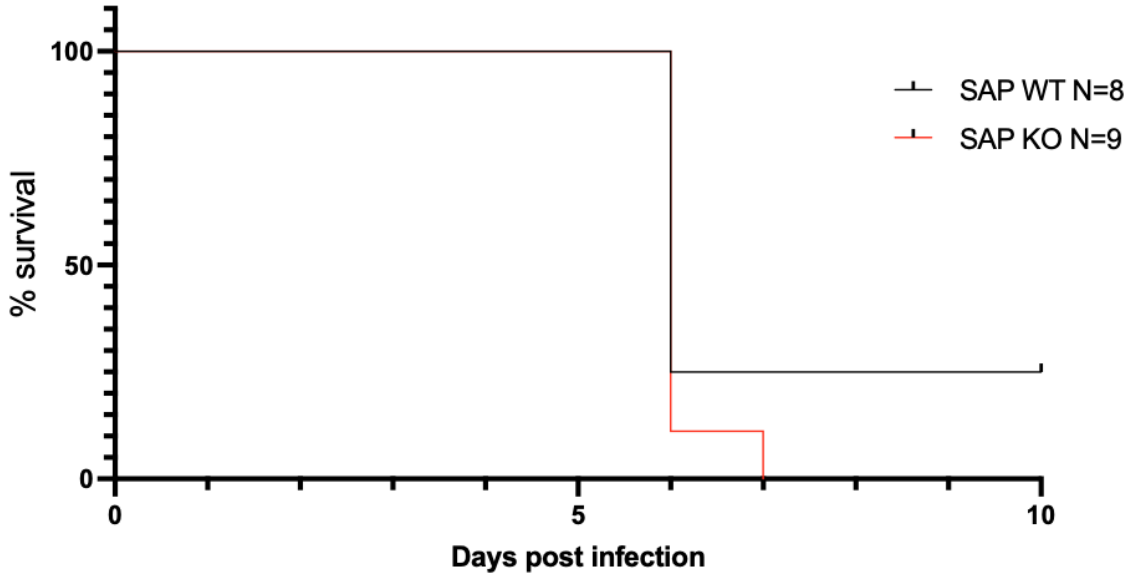

Supplementary Figure 2: No significant difference in survival between SAP KO and WT female mice infected with low dose. Results shown are pooled from two independent experiments. The red line represents SAP KO mice and the black line represents SAP WT mice.

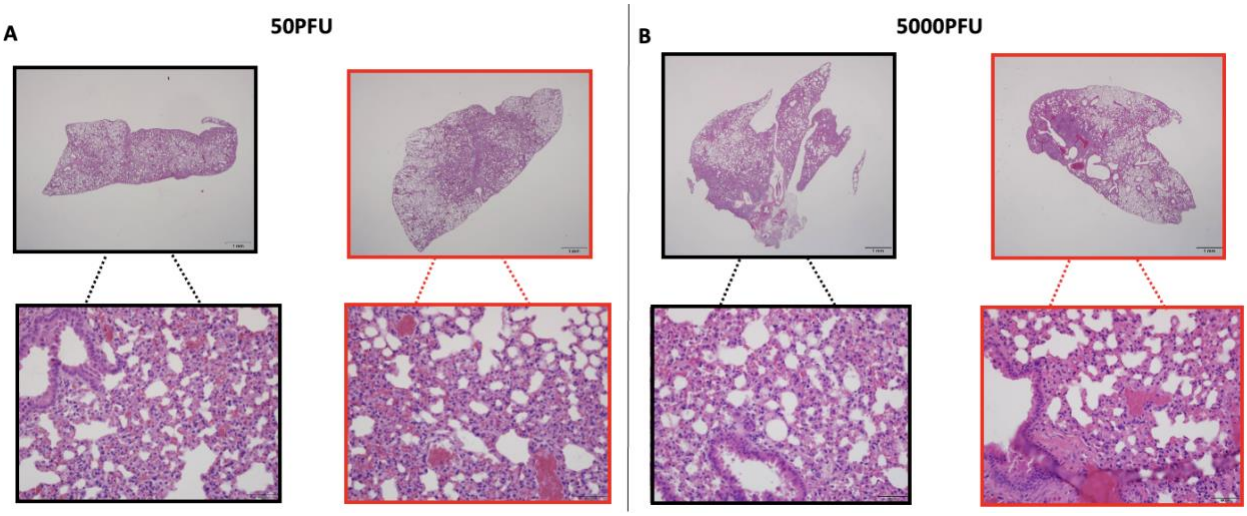

Supplementary Figure 3: Histopathological Findings. (A) Representative images of H & E stained half lungs obtained from SAP WT and SAP KO infected mice with low dose (50 PFU). (B) Representative images of H & E stained half lungs obtained from SAP WT and SAP KO

infected mice with medium dose (5000 PFU). Black squares are indicative of samples from SAP WT mice; and red squares are indicative of samples from SAP KO mice. The top images are shown at a magnification of 1mm and the images at the bottom are shown at a magnification of 50um.

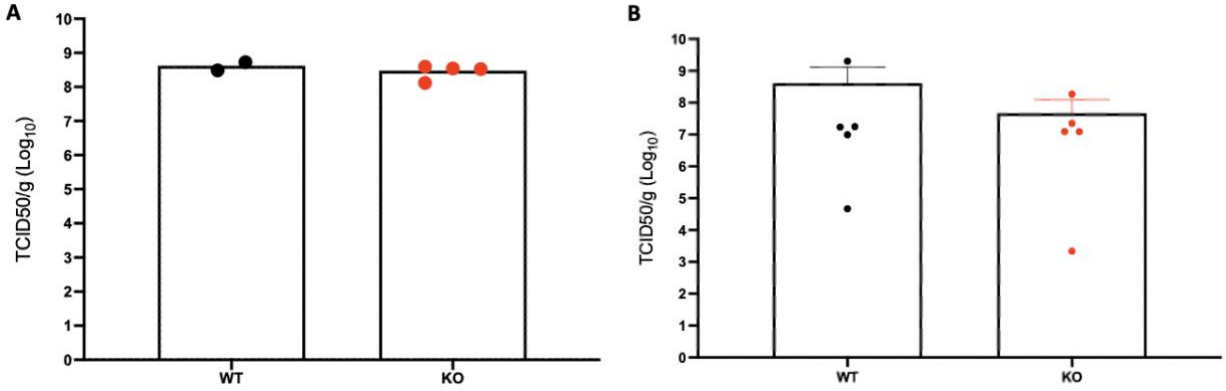

Supplementary Figure 4: No difference in infectious viral titre in the brain between SAP WT and KO infected mice. (A) The virus titre in the brain of mice infected with low dose (50 PFU) is shown for SAP WT (black, n=2) and SAP KO (red, n=4). (B) The virus titre in the brain of mice infected with medium dose (5000 PFU) is shown for SAP WT (black, n=5) and SAP KO (red, n=5).

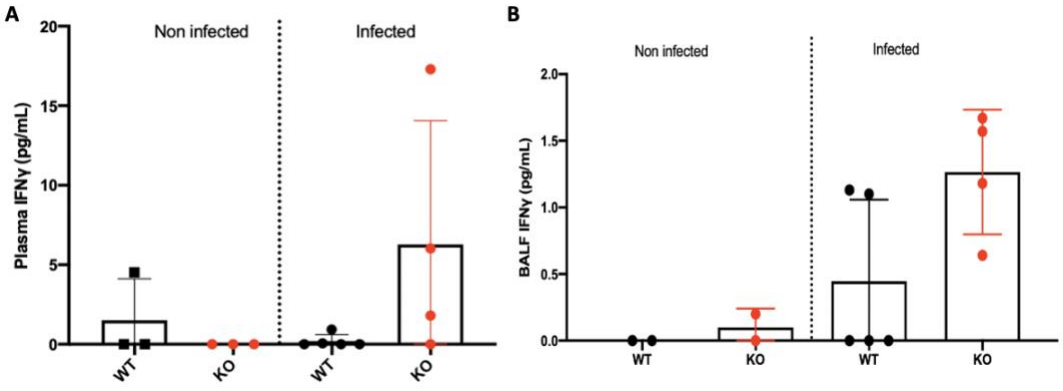

Supplementary Figure 5: Trend of increase of plasma and BALF IFNγ in infected SAP KO mice compared to SAP WT. (A) Plasma IFNg levels from medium dose (5000 PFU) infected SAP KO

(n=4) and SAP WT (n=5), as well as non-infected controls (n=3 for each) at 5 DPI. BALF IFNg levels from high dose (25000) infected SAP KO (n=4) and SAP WT (n=5), as well as non-infected controls (n=2 for each). Units on the y axis are displayed as picograms/mL (pg/mL). Red dots are SAP KO and black dots are SAP WT mice.

Gene	Sense Primer (5'-3')	Antisense Primer (5'-3')	Product size (bp)
shd2d1a	GGTCAACACTTTAACATGTTAG	CACTATAAGTTACACATGGTCC	1039
Chr2 (linked to (K18-ACE2)2Prlmn)	TGTTGGAACTTTGTGCTTGG	AACAGATGTCAAATAGGACAACAC	285
SARS-CoV-2 Spike	GGCAGAGACATTGCTGACAC	AGCAACAGGGACTTCTGTGC	174
Gapdh	ACCACAGTCCATGCCATCAC	TCCACCACCCTGTTGCTGTA	452
Ifnγ	CAGCAACAGCAAGGCGAAAAAGG	TTTCCGCTTCCTGAGGCTGGA	2503
Gzmb	TGCTGACCTTGTCTCTGGCC	TAGTCTGGGTGGGGAATGCA	1512
Prf1	AGCACAAGTTCGTGCCAGG	GCGTCTCTCATTAGGGAGTTTTT	151
Cd8α	CCGTTGACCCGCTTTCTGT	CGGCGTCCATTTTCTTTGGAA	121
Nkp46	TAGGGCTCACAGAGGGACATAC	GTAGGTGCAAGGCTGCTGTTCT	333

Supplementary Table 1: List of primers used for genotyping mice and assessing gene expression.

Nucleotide Position	Nucleotide Change	Type of Mutation	Protein/UTR region	Amino acid change
241	C->T	upstream gene variant	5'UTR	-
3037	C->T	synonymous variant	Nsp3	F106F
5422	T->C	synonymous variant	Nsp3	N901N
14408	C->T	missense variant	Nsp12b	P314L
15324	C->T	synonymous variant	Nsp12b	N619N
21784	T->A	missense variant	S	N74K
23403	A->G	missense variant	S	D614G
23607	G->A	missense variant	S	R682Q
24433	C->T	missense variant	ORF3a	T14I

Supplementary Table 2: List of all consensus mutations and amino acid changes of our virus stock relative to the Wuhan-Hu-1 NC_045512 sequence.

SARS-CoV-2 Clinical Scoring

Appearance	
Ruffled fur (normal = 0; mild = 1; moderate = 2)	**Hunching** (normal = 0; mild = 1; moderate = 2; severe =3)
Activity	**Specific Signs (dyspnea)**
Locomotion/mobility: active = 0; less active = 1; moderately less active = 2; lethragic = 3	normal = 0; mild (increased respiration rate when active) =1; moderate (increased respiration rate at rest)=2; severe (labored breathing) = 3

Clinical Endpoint
Total Score of >10
BW loss > 20%
Body condition < BC2
Inactivity

Supplementary Table 3: Guidelines for scoring severity of infection and to guide humane euthanasia endpoint (or clinical endpoint).